6 Magnetic Resonance Imaging and Analysis in Multiple Sclerosis

Dejan Jakimovski, Deepa P. Ramasamy, and Robert Zivadinov

Introduction

Multiple sclerosis (MS) is regarded as a chronic autoimmune demyelinating disease of the central nervous system (CNS), affecting more than two million people worldwide [1]. The multifocal demyelinated plaques seen on magnetic resonance imaging (MRI) appear throughout the CNS and are characterized with areas of focal inflammation, edema, glial reaction, and scarring. In the early stages of the disease, the acute appearance of the focal lesions is commonly accompanied with episodes of intermittent and accumulating neurological dysfunction [2]. Although MS still remains incurable, the early use of more than dozen available disease-modifying therapies allows fewer acute neurological episodes, lowers the MRI-detected pathological changes, and delays the accumulation of long-term physical disability [3].

Even though the conventional MRI is 5–10 times more sensitive than clinical examination in assessment of the MS disease activity, the technique has a number of drawbacks that limit the reliability as an overall surrogate marker for detecting clinical progression [4]. The unsuccessful efforts to link the MRI-derived markers and the clinical disability scores have resulted in the coinage "clinical-radiologic" paradox [5]. Although the current gap between the clinical-radiologic paradox has been substantially reduced over the last decade, the overall MRI correlations still remain modest at best [6]. Therefore, this review will outline the major strengths and limitations of the conventional and nonconventional MRI techniques in their attempt to detect the inflammatory and neurodegenerative aspects of MS.

D. Jakimovski · D. P. Ramasamy · R. Zivadinov (✉)
Department of Neurology, Buffalo General Hospital, University of Buffalo, Buffalo, NY, USA
e-mail: djakimovski@bnac.net; dramasamy@bnac.net; rzivadinov@bnac.net

Conventional MRI in Multiple Sclerosis

MS Lesion Detection

Currently, there is no consensus on the precise and specific definition for the white matter (WM) hyperintensities (hereafter referred only as lesions) that are commonly seen in MS patients. Although variable, the MS lesions are usually ovoid or round in shape and are centered on small penetrating vessels. Their occurrence in the periventricular WM, juxtacortical, and infratentorial region is a relatively specific sign for MS. When imaged on sagittal MRI views, the ovoid lesions of the corpus callosum have typical radiographic appearance termed "Dawson fingers." The characteristic decay of the nuclear spin is called transverse relaxation (T2) and it describes the time it takes for the signal to decrease to the 63% of its original value [7]. Among many variations

S. A. Rizvi et al. (eds.), *Clinical Neuroimmunology*, Current Clinical Neurology,
https://doi.org/10.1007/978-3-030-24436-1_6

between sequences that are able to detect the T2 changes, the most often recommended are: conventional echo, fast spin-echo (FSE), turbo spin-echo (TSE), and fluid-attenuated inversion recovery (FLAIR) [8]. T2-weighted imaging (WI) allows highly specific detection of the disease activity and the lesion appearance over time; however, it has intrinsic limitation in the ability to distinguish between the differential substrates of the T2-WI hyperintensities (inflammation, edema, demyelination, and axonal loss). Compared to higher sensitivity of the FLAIR sequence in detecting subcortical and discrete cerebral lesions, the FSE proton-density (PD) imaging allows better and more accurate detection of focal lesions within the infratentorial compartment [9]. Based on their appearance under different MR sequences, the majority of MS lesions are classified into three main groups: T2 hyperintense, chronic T1 hypointense (also known as "black holes"), and gadolinium (Gd) enhancing lesions on post-contrast T1-WI (Fig. 6.1).

Apart from the symptomatic lesion, clinically isolated syndrome (CIS) patients tend to exhibit multiple asymptomatic brain lesions even before their first onset clinical presentation (radiologically isolated syndrome, RIS). The number of T2 hyperintense lesions is directly associated with the percentage and the time of reaching clinically definite MS diagnosis (81% of patients with ≥10 lesions when compared to only 9% in patients with an absence of T2 lesion, hazard ratio (HR) of 19.7) [10]. Similarly, the baseline T2 characteristics have the highest predictive value for detecting patients that will reach an Expanded Disability Status Score (EDSS) of 3.0 (22% of patients with ≥10 lesions when compared to only 4% in patients with absence of T2 lesion, HR of 4.4) [10]. The role of MRI-derived inflammatory biomarkers as high-impact prognostic factor have been also carefully studied and demonstrated within the initial large interventional MS trials [11]. Greater baseline MRI lesion volume and greater increase of lesion volume over time are moderately associated with clinical disability after 20 years [12]. Within this long-term follow-up, the rate of the lesion volume accumulation is substantially higher in patients that develop secondary progressive MS (SPMS) than in patients who maintain their relapsing–remitting MS (RRMS) status (2.89 cm^3/year vs. 0.80 cm^3/year) and this difference is already evident within 5 years of disease presentation [12].

The lack of specificity and the moderate correlations with the clinical disability call for improvement of the quality of T2-WI sequences

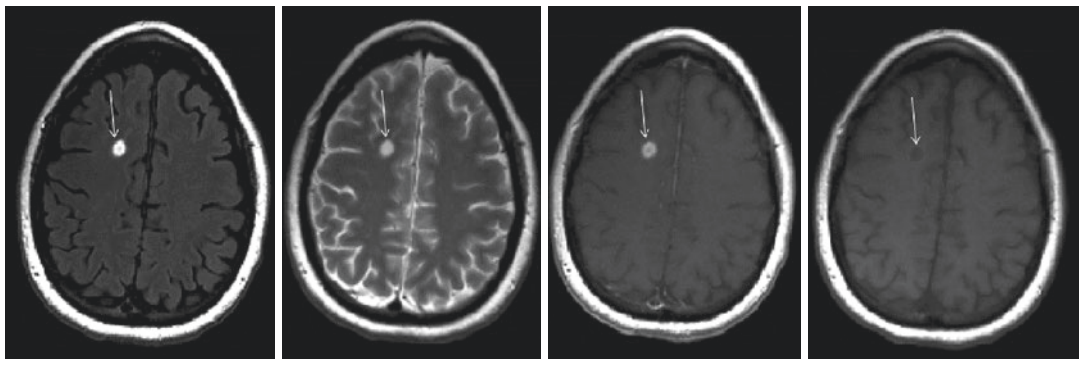

Fig. 6.1 T1-weighed imaging, T2-weighted imaging, FLAIR, and gadolinium enchanced T1-weighted imaging. Conventional magnetic resonance imaging in multiple sclerosis patient including: (**a**) 2D fluid-attenuated inversion recovery (FLAIR) sequence, (**b**) T2-weighted image (WI) sequence, (**c**) T1-WI post-contrast sequence, and (**d**) T1-WI pre-contrast sequence. The contrast enhancing lesion (white arrow) seen on the T1-WI post-contrast correlates with hispathological findings of blood-brain-barrier (BBB) breakdown and acute inflammation. Note the initial hypointensity of the acute MS lesion on the pre-contrast 2D T1-WI image

and use of additional quantitative approaches that will better characterize the lesions. The use of thinner 2D FLAIR slices (1.5 mm) can increase the sensitivity for detection of cortical and juxtacortical lesions in MS patients [13]. Lesion detection can be also substantially increased with the application of 3D MRI techniques, which provide equal spatial resolution along all three different axes. 3D FLAIR imaging uses inversion recovery preparation with variable flip angles that establishes pseudo-steady-states/relaxation contra-balancing, and allows nonblurred images despite the long echo trains. Although initially 3D FLAIR showed significant increase in the ability to detect MS lesions, the sequence required long, clinically unfeasible scanning times [14]. The 1.7 times increase in number of lesions detected by the single-slab 3D FLAIR when compared to the conventional 2D FLAIR may be also attributed to the significantly higher contrast-to-noise ratio (Fig. 6.2) [15]. However, recent optimization of the sequence parameters retained the increase in detection of both supra- and infratentorial lesions within acceptable reduction of the scanning time [16]. Despite the fact that many groups have tried to develop an automated and unsupervised method for MS lesion segmentation, thus far, these techniques are not readily available for wide clinical use [17].

The seminal paper by Trapp et al. demonstrated that the active inflammation during the demyelinating process causes a large number of axonal transections [18]. As a consequence of this acute focal axonal transection, the signal intensity within 80% of the active lesions shows initial T1-WI hypointensity [19]. As the inflammation subsides, 40% of the T1-WI hypointensities undergo process of remyelination, tissue repair, and return to their isotense signal characteristic [19]. However, the remaining percentage of acute black holes continues to degrade and develop into persistent black holes. The assessment of the persistent black holes was considered as the first measurable biomarker of the neurodegenerative process in MS [20]. Moreover, the presence and the extent of black holes have been repeatedly shown as one of the best predictive factors for disability in long-term follow-up studies [21, 22].

Gd enhancement is a transient phenomenon of the MS lesion that correlates with histopathological findings of blood-brain-barrier (BBB) breakdown and acute inflammation. When compared to T2-derived lesions, the Gd enhancing lesions are typically easier to identify and are less dependent on technical factors like acquisition parameters and intra- and interobserver variability. Due to the short interval of Gd persistence (3–6 weeks), the enhancing lesions may

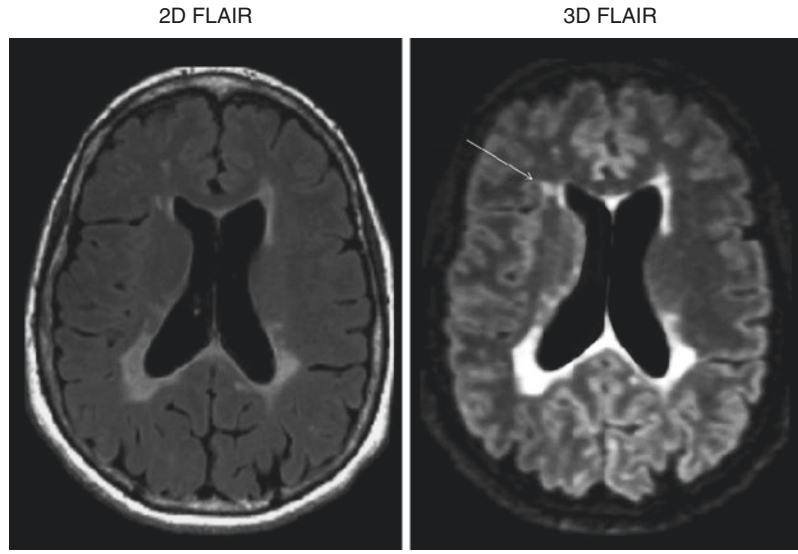

Fig. 6.2 Lesion detection comparison between 2D FLAIR and 3D FLAIR sequences. In addition to the improved lesion to noise contrast ratio, the 3D FLAIR image provides better delineation of white versus gray matter and allows detection of cortical lesions (white arrow)

remain undetected by the regular 3–6 month rescan periods. Therefore, Gd enhancing lesions are not sufficiently sensitive as singular measures of disease activity and treatment evaluation. In response to this limitation, in order to detect patients with suboptimal treatment response, several proposed scoring methods or criteria combine the clinical and MRI-derived measures [23]. In particular, the purposed scoring systems like the Rao scale, the modified Rao scale, and the European Medicines Agency (EMA) criteria showed variable sensitivity and specificity in detecting patients that will exhibit increased relapse rate or/and disability progression (ranging between 24% and 71% sensitivity and 71–97% specificity) [23]. A recent composite that included both absence of clinical and radiographic activity was initially termed "disease activity free status" (DAFS) and later renamed as "no evidence of disease activity" (NEDA). Although it has been shown that achieving and sustaining long-term NEDA status is especially difficult, NEDA has the potential to become a key therapeutic target goal in the future [24].

Both acute enhancing and chronic non-enhancing MS lesions show time-dependent increase in contrast enhancement [25]. The greater contrast enhancement seen in scans acquired after longer delay from the Gd administration suggests persistence of BBB leak [25]. Furthermore, several studies have shown that application of Gd would intensify the T1 effect on the FLAIR images and improve the detection of extra-axial pathology and meningeal enhancement [26]. Therefore, a combination of delayed post-contrast imaging and use of 3D FLAIR sequence allowed illustration of leptomeningeal contrast enhancement (LM CE) adjacent to the cortex of MS patients [27]. The aforementioned LM CE has been documented by several research groups and has been associated with patient age, disease severity, and the clinical type of MS [28]. A postmortem 7 T and histopathological examination of the structures that present as LM CE on MRI demonstrated that the aggregates of T- and B-cells are organized within a tertiary follicle-like structure [27]. The surrounding cortex of the sulcus that hosts the tertiary follicle-like structure also shows extensive cortical demyelination [27]. Furthermore, the presence of LM CE was associated with lower global gray matter (GM) and cortical volume [29]. A similar 7 T MRI examination additionally showed that only a specific pattern of spread/fill foci are associated with the reduced cortical GM volumes, whereas the nodular foci may represent a normal variant [30]. Figure 6.3 exhibits the utility of post-contrast FLAIR in detecting the LMCE and demonstrates the differences between nodular versus spread/plate-type of LMCE. The proximity of the aforementioned tertiary follicle-like structures may potentially link the meningeal inflammation with the type III subpial cortical lesions. With the introduction of the new B-cell depleting therapies for MS, better understanding and reliable detection of the LM CE could potentially become a useful biomarker in assessing their therapeutic efficacy [31].

In contrast to the 3D FLAIR, the three-dimensional double inversion recovery (3D DIR) uses additional radiofrequency (RF) pulse that results in suppression of both the WM and the cerebrospinal fluid (CSF) [7]. The additional inversion pulse used in DIR imaging proves to decrease the signal-to-noise ratio and make the images appear noisier; however, it provides excellent contrast-to-noise ratio between the lesion and the parenchyma and may be an excellent tool for detecting cortical lesions (Fig. 6.4). The cortical lesions can be detected throughout all MS phenotypes and are mainly grouped as leukocortical or type I (lesions that extend through both GM and WM), intracortical or type II (lesions exclusively within the GM), and subpial or type III (lesions abutting the pia and extending into the cortex) [32]. Furthermore, DIR has been used for imaging of the optic nerve, the infratentorial segment, and the spinal cord. The DIR showed improved sensitivity at detecting lesions with a 7% gain with respect to FLAIR and 15% gain with respect to T2-WI [33]. The increase was even larger in respect to the infratentorial lesions with 56% increase when compared to FLAIR and 44% increase when compared to T2-WI [33]. In longitudinal examinations, DIR subtraction maps improved the detection of new and enlarged lesions both in terms of accuracy

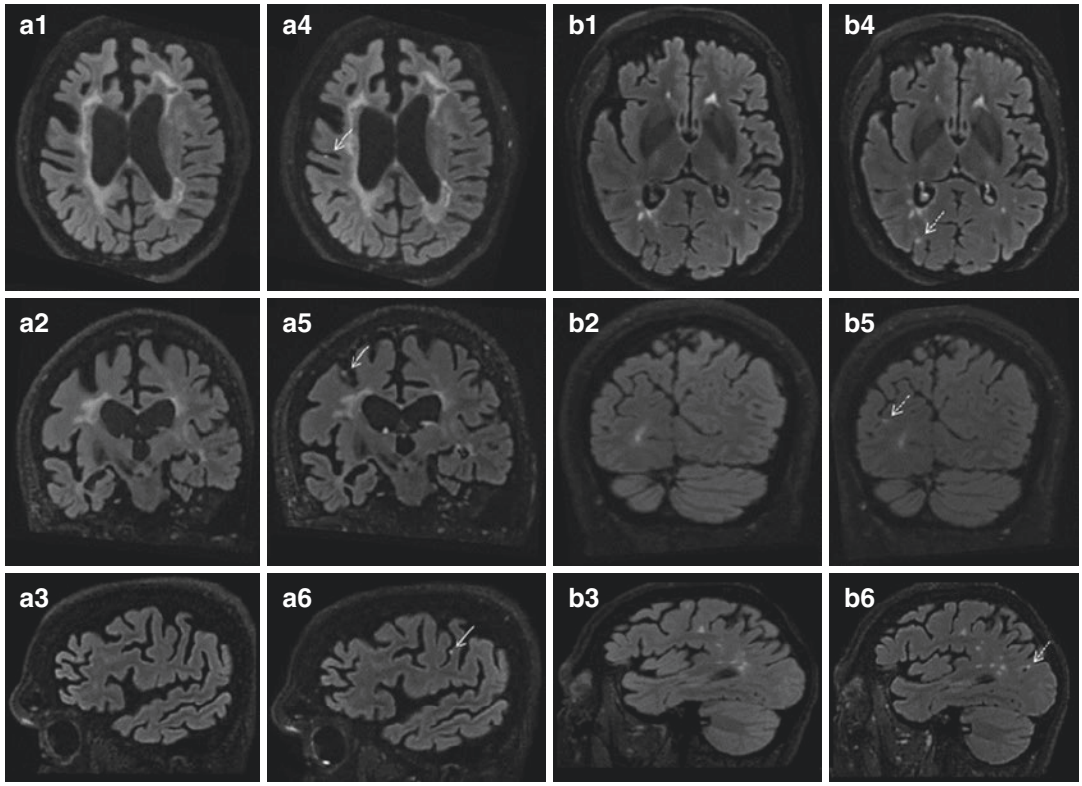

Fig. 6.3 Leptomeningeal enhancement in multiple sclerosis patients. The use of pre-contrast (**a**1–3 and **b**1–3) and post-contrast (**a**4–6 and **b**4–6) 3D fluid-attenuated inversion recovery (FLAIR) sequences in detection of leptomeningal contrast enhancment (LMCE). Sixty-three-year-old secondary progressive multiple sclerosis patients presenting with nodular LMCE enhancement (white arrow) demonstrated in all plane post-constrast 3D FLAIR images. Fifty-seven-year-old relapsing–remitting multiple sclerosis patients presenting with "spread/plate"-like LMCE (dotted white arrow)

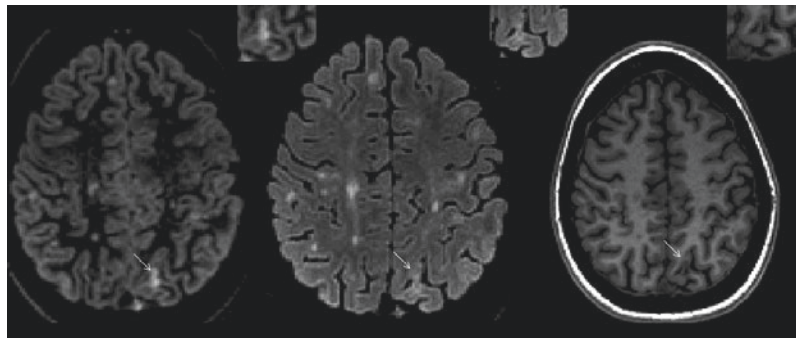

Fig. 6.4 Cortical lesion imaging using double inversion recovery (DIR) sequence. Double inversion recovery (DIR) sequence uses two separate radiofrequency pulses that suppress both the white matter and the cerebrospinal fluid signal. The sequence allows better detection of cortical lesions (white arrow) when compared to conventional sequences. (**a**) Double inversion recovery (DIR) sequence, (**b**) fluid-attenuated inversion recovery (FLAIR) sequence, and (**c**) fast spoiled gradient echo (FSPGR) sequence

and the time needed for the scan read [34]. The reported 1.7 times more detected active lesions using DIR subtraction was mainly driven by the strength of the DIR sequence in detecting cortical lesions [34]. The same group also demonstrated that post-contrast DIR imaging can detect significantly more (16%) contrast-enhancing lesion when compared to the traditional post-contrast T1-WI [35]. Despite the comparative improvement to the conventional FLAIR imaging, the 3D DIR technique is still not able to detect up to 80% of the cortical lesions seen under microscope [36]. The latest consensus recommendations for cortical lesion scoring using the DIR sequence included that (1) the GM lesions should be clearly hyperintense on DIR and (2) should cover at least three pixels based on minimal in-plane resolution of 1.0 mm^2 [37]. This recommendation also takes into account the relatively noisier 1.5 T DIR images when compared to 3 T. Due to the high association of cortical lesion load with physical and cognitive progression, the ability to successfully image the cortical pathology may help in early identification of patients with the most severe prognosis [38].

The latest guidelines published by the European Magnetic Resonance Imaging in MS (MAGNIMS) network recommended a standardized protocol for baseline and follow-up MRI examinations for patients with suspected or clinically definite MS [39]. The baseline examination included mandatory use of axial proton-density (PD) and/or T2-FLAIR/T2-WI, sagittal 2D or 3D FLAIR, and a 2D or 3D contrast-enhanced T1-WI. Additional (optional) sequences included unenhanced 2D or high-resolution 3D T1-WI, 2D and/or 3D DIR sequence, and an axial diffusion-weighted imaging (DWI) sequence. Similarly, the follow-up MRI examinations should include at least the mandatory PD or T2-FLAIR and the 2D or 3D contrast-enhanced T1-WI, with optional addition of the high-resolution 3D T1-WI, 2D/3D DIR, and axial DWI. Unfortunately, the minimum recommended milieu of sequences is not able to provide reliable prognostic information for establishing disease progression. The addition of repeat scans within the first few months of treatment initiation can considerably predict the treatment response [23]. Additionally, the use of automated subtraction techniques (follow-up vs. baseline subtraction) can improve the accuracy and sensitivity of detecting new and/or enlarging T2 lesions [23]. As discussed later in this review, the current data still does not support the use of automated brain volume nor spinal cord measures in predicting the individual treatment response rate [23].

MRI Contrast Agents and Contrast Deposition

The fundamental capability of contrast agents to efficiently lower the relaxation times of T1 and/or T2 allows generation of better MRI-derived signal and better detection of lesions. The addition of paramagnetic ions like gadolinium (Gd^{3+}), iron ($Fe^{2+,3+}$), and manganese (Mn^{2+}) act as individual microscopic magnets that cause faster neighboring proton relaxation back to their equilibrium state. In comparison to Gd, the iron-based agents have stronger ability to affect the relaxation times and they are mostly used as dark MRI contrast (T2∗ imaging). These iron oxide particles vary in size, from ultrasmall superparamagnetic particles of iron oxide (USPIOs, 5–50 nm) to superparamagnetic iron oxide particles (SPIOs, 50–150 nm) and micron-sized iron oxide particles (MPIOs, ≈1 μm) [40].

A major benefit in utilization of USPIOs in imaging of the inflammatory diseases like MS is their ability to be captured by the circulating monocytes/macrophages and travel to the site of inflammation. Thus, USPIO contrast agents are able to provide higher cell specificity and better understanding of the CNS inflammation. Additionally, potential coupling of MPIOs with anti-adhesion antibodies can provide direct imaging of endothelial surface markers (E-selectin and P-selectin) that control immune cell trafficking [41, 42]. The discrepancies of contrast enchantment seen while imaging with both USPIOs and Gd-based agents have suggested an active monocyte infiltration through the preserved integrity of the BBB [43]. However, the appearance of USPIO within an hour of its administration points to a

second, cell-independent transport indicates leaky BBB [44]. On that note, USPIO-related abnormalities can be already seen at day 10 after EAE disease induction, a period which does not include macrophage infiltration [44]. The later process of passive USPIO diffusion is cleared through neighboring cervical lymph nodes and does not produce significant contrast changes after 24 h of administration [44]. Therefore, knowledge about the USPIO kinetics is crucial in determining the temporal and mechanistic characteristic of USPIO imaging.

Due to the ionic radius of 0.99 Å, Gd in its stable oxidation state (Gd^{3+}) can easily compete for the binding sites of Ca^{2+} and produce relative biological toxicity. Prior to its use in humans, the Gd requires a process of chelation that will prevent free Gd^{3+} circulation [45]. Generally, the current Gd-based MRI contrast agents (GBCAs) are divided into four types: macrocyclic or linear and they can be additionally separated as ionic (charged) or non-ionic. The particular chemical structure produces inherent differences in the kinetic stability [46]. In presence of endogenous cations like Cu^{2+} or Zn^{2+}, the linear agents can exhibit poorer kinetic stability and dissociate [46].

A potential association of MRI-detected brain abnormalities and previous exposure to linear chelate GBCAs has been initially published in 2014 [47]. It showed a positive correlation between high signal intensity of the dentate nucleus and history of multiple GBCA administrations [47]. These preliminary results were later confirmed with GBCA accumulation studies in patients with MS, brain metastasis, and in pediatric population [48]. A preclinical study investigated the amount of Gd deposition in rat brains after 20 consecutive injections of linear GBCA, macrocyclic GBCA, or placebo [49]. The results corroborated that linear GBCA leads to progressive increase in MRI signal intensity ratio [49]. Additionally, postmortem autopsy demonstrated higher amount of linear GBCA deposition when compared to rats exposed to the macrocyclic GBCA or placebo [49]. A similar study examined multiple formulations of GBCAs and showed that all three linear GBCAs tested had significantly higher brain deposition than placebo or the macrocyclic GBCAs [50].

Until recently, the only other known adverse effect related to Gd administration was a rare nephrologic condition called nephrogenic systemic fibrosis. Due to the aforementioned reports of Gd deposition in the brain, the FDA issued warning, which suggests avoiding linear GBCAs administration if not necessary. The highest retention was seen among the linear gadodiamide (Omniscan®) and gadoversetamide (OptiMARK®), followed by gadopentetate dimeglumine (Magnevist®), gadobenate dimeglumine (MultiHance®), and gadoxetate disodium (Eovist®), and the lowest retention with the use of the macrocyclic gadoterate meglumine (Dotarem®), gadoteridol (ProHance®), and gadobutrol (Gadavist®). Additionally, the EMA suspended the use of the aforementioned Omniscan®, Magnevist®, OptiMARK®, and restricted the use of MultiHance® only for liver scans. In conclusion, convincing evidences demonstrate active deposition of Gd in the deep brain nuclei, particularly after repeated linear GBCAs exposure. The biological and clinical effect of this brain deposition still remains undetermined in patients with MS and other diseases [51].

2017 Revision of McDonald Criteria for Multiple Sclerosis Diagnosis

Due to the rapid growth of the medical imaging field, periodical revision of the diagnosis guidelines would provide continuous improvement in the sensitivity and specificity of the criteria [52–54]. The new 2017 revision of the MS McDonald criteria has focused on clarifying and simplifying the constituents of the previous versions, changes that will ultimately allow lower frequency of MS misdiagnosis [54]. The previous 2010 revision of the McDonald criteria required that dissemination in space (DIS) should be demonstrated by ≥1 T2 lesion in at least two of four areas of the CNS (periventricular, juxtacortical, infratentorial, and spinal cord). On the other hand, for the demonstration of dissemination in time (DIT), it required: (1) a new T2 and/or Gd enhancing lesion on follow-up MRI or (2) simultaneous

presence of asymptomatic Gd enhancing and non-enhancing lesions at any time [53].

The first step into improving the CIS/MS classification was the inclusion of the CSF-derived oligoclonal bands (OCB) as acceptable substitute for the DIT requirement. The change was prompted by multiple recent studies showing that presence of CSF OCB is an independent predictor of consecutive second attack [10, 55]. In a large multicenter study, the presence of OCB was associated with increased conversion to MS (hazard ratio of 2.18) [56]. Furthermore, a meta-analysis showed that the presence of OCB in the CSF of CIS patients resulted in increased chance (odds ratio of 9.9) of conversion to MS [57].

As a second amendment, the new criteria remove the discrimination between symptomatic and asymptomatic T2 lesions in the determination of DIS or DIT [58, 59]. The previous distinction was done with an idea to exclude the symptomatic lesion from the required two out of four MS characteristic region involvement (periventricular, juxtacortical, infratentorial, and spinal cord) and prevent double counting. As an example, a patient presenting with an acute partial transverse myelitis would require only one or more T2-hyperintense lesions in the remaining three regions (paraventricular, juxtacortical, or infratentorial) in order to fulfill the new 2017-revised McDonald criteria. Although still debated, lesions in the optic nerve are considered as exception from this rule and still remain insufficient in documenting DIS or DIT [60, 61].

Lastly, the new 2017 McDonald criteria recommend the inclusion of cortical lesions as equal constituents for fulfilling the DIS requirement. The ability to routinely and reliably detect cortical lesions requires additional MRI sequences that were previously described in this review. The expert panel of the revised 2017 criteria has recognized the potential imaging artifacts and the current limitations of DIR imaging [62, 63].

The future alliterations of the MS diagnosis guidelines should focus on defining entities like RIS, solitary sclerosis, *possible multiple sclerosis*, pediatric multiple sclerosis, anti-MOG pathology, and the diagnosis of MS in more diverse populations [64–66]. Future standardization of the nonconventional techniques like multi-echo MRI imaging, GM imaging, optical coherent tomography (OCT), evoked potentials, and laboratory tests may increase the accuracy of the diagnosis.

Spinal Cord Imaging

Due to the inclusion of the spinal cord region as part of the four areas included in the McDonald criteria, spinal lesions can be used to demonstrate DIS. Therefore, spinal cord imaging is an essential diagnostic tool that should be obtained in patients with spinal cord symptomatology and patients in whom brain scans do not solemnly fulfill the McDonald criteria for MS diagnosis [67]. The spinal cord MRI abnormalities are not exclusively seen in MS and should be differentiated from diseases like neuromyelitis optica spectrum disorder (NMOSD), myelin oligodendrocyte glycoprotein myelopathy (anti-MOG disease), and idiopathic transverse myelitis (ITM) [68]. Regardless of the OCB and brain MRI findings, the spinal cord lesions independently contribute to two- to threefold increase in risk for reaching an MS diagnosis [69]. Indeed, even in patients with non-spinal CIS presentation, the detected spinal cord MRI abnormalities are able to explain a larger amount of follow-up disability progression when compared to the brain MRI measures [70]. Both the accumulation of asymptomatic spinal cord lesions and the progression of spinal cord atrophy in CIS patients contribute up to 50% of the MS-related disability accumulation over mid-term follow-up period [70].

Most spinal cord scans were traditionally acquired with the use of sagittal dual echo (PD and T2) sequence. Together with the increasing clinical 3 T availability, multiple combination of sequences have been purposed to increase the lesion detection and regional cord volume detection. For example, sequences like short tau inversion recovery (STIR) and phase-sensitive inversion recovery (PSIR) use fat suppression and allow better spinal cord lesion assessment and WM versus GM separation [71]. Multiple findings demonstrate that the preferential loss of

spinal cord GM is associated with more severe EDSS score and walking disability, whereas spinal cord WM did not [71, 72]. Manual and automated models of spinal cord volume segmentation have been additionally proposed [73].

The relationship between spinal cord pathology and the disability progression has been especially emphasized within SPMS and primary progressive (PP) MS patients [74]. In a large single-center retrospective study, all SPMS patients and almost all PPMS had spinal cord lesions at their C2–C3 level [74]. Additionally, PPMS patients had significantly more spinal cord atrophy when compared to SPMS and healthy controls [74]. The overall sample size calculations for the use of spinal cord cross-sectional area measurement in PPMS patients resulted only in 57 subjects per arm needed, whereas for SPMS it required at least 546 subjects per arm [74]. Therefore, future PPMS and neuroprotective MS trials should consider spinal cord imaging as part of their outcome measures.

The use of nonconventional spinal cord MRI studies are still in their very early stages and have relatively limited clinical applicabilty [75]. DTI of the spinal cord (FA metric) is the only nonconventional technique that provides moderate evidence of association with impairment in a number of neurological diseases [75]. The larger magnetic field inhomogeneity and the intensified intrinsic motion caused by the cardiac and respiratory cycles remain as major limiting factors in the acquisition of high-quality spinal cord data [70].

Ultra-High-Field MRI Imaging in MS

The advantages and limitations of ultra-high-field imaging can be essentially explained by the increase of the main magnetic field (B_0). The larger initial amount of spins that are transversely aligned with the magnet will produce larger net magnetization. However, the larger strength will also introduce a larger B_0 inhomogeneity that can cause artifacts and signal loss. When compared to 1.5 T and 3 T MRI imaging, the 7 T scanners allow five- to tenfold increase of the signal-to-noise ratio. Additional benefits of ultra-high-field MRI imaging are: improved contrast derived from the magnetic susceptibility variations, greater chemical shift dispersion, and faster echo planar imaging. The 7 T MRI scanners have been extensively used in understanding the pre-lesional WM changes, evolution of the cortex changes, detection of GM lesions, and understanding the process of neurodegeneration [76]. The increased number of WM lesions detected with the ultra-high-field MRI systems suggests that the current imaging protocols are not fully capturing the MS pathology [77]. Additionally, the higher imaging resolution provides improvement in the differential diagnosis of WM abnormalities and in their differentiation from other mimicking demyelinating lesions [78–80]. Several studies have shown that 7 T imaging allows more than double increase in the detection rate of cortical lesions in MS [62, 81, 82]. However, when compared to histopathological analysis, up to 40% of the subpial (type III) cortical lesions are still missed even at 7 T MRI [62]. Similarly, a study using 7 T, T2∗ MRI sequence produced surface-based analysis that showed in vivo characterization of the degree of cortical pathology at different depths of the cortex [83]. The gradient in the intracortical pathology across different disease stages demonstrates that the pathology is driven from the pial surface itself [83]. As of October 12th, 2017, the FDA approved human clinical use of the first 7 T MRI device (Magnetom Terra®, Siemens), which allows for 0.2 mm in-plane resolution, voxel size of 0.14 cm^3, and submillimeter fMRI BOLD signal specifications.

Nonconventional Imaging

Brain Atrophy

The physical and cognitive decline seen in the later stages of the disease are not represented by the sparse MRI-detected inflammatory lesions. The purposed two-stage process might potentially explain the failure of the current anti-inflammatory therapeutics in their ability to

control the secondary inflammation-independent disability progression [84]. The underlying brain atrophy seen throughout all stages of MS can be generally explained by three main subsequent pathological processes: tissue loss within the lesions themselves (T1-hypointensities), Wallerian degeneration affecting the length of the transected axons, and independent neurodegenerative changes within the NAWM and NAGM [18]. As the axons do lose their myelin sheath, a compensatory upregulation of sodium channel expression sustains the signal transduction [85]. Intensified sodium channel usage requires greater amount of ATP that eventually gets depleted and induces mitochondrial dysfunction [85]. The mitochondrial dysfunction further causes global neuronal energy deficit and cascades to toxic accumulation of Ca^{2+}, which finally leads to neuronal death [85]. Potential inhibition of the specific $Na_v1.6$ channels might prevent the "inside-out" pathophysiology of the MS neurodegeneration [86]. The robustness of the ongoing axonal loss has been documented with histological analysis of the cerebrospinal tract [87]. After a lifetime of MS (an average of 30 years of disease duration), the corticospinal tract loses approximately 60% of the total axonal pool [87]. Similarly, the normal-appearing white matter (NAWM) demonstrates substantial loss (50%) of both axon density and volume [88].

On the other hand, the GM atrophy is primarily affected by neurodegeneration, a co-occurring process that is not associated with presence of GM lesions, the overall myelin density, or the survival of the oligodendrocytes [89]. The first systematic histopathological and MRI investigation showed that the cortical volume in long-lasting MS patients is largely and independently explained by neuronal density, neuronal size, and axonal density [90]. After a mean disease duration of 27 years, MS patients have almost 40% less total number of neocortical neurons and almost 30% reduction in neuronal density when compared to controls [91]. This neuronal loss was seen in all lobes investigated with the exception of the primary occipital (visual) cortex. The association between the overall neuronal loss and the MRI-derived cortical volume demonstrates that in vivo MRI studies can provide robust prediction of cortical pathology [91].

A serial yearly MRI scans acquired over a decade showed that ventricular CSF space and the whole brain atrophy in early MS patients can predict the development of disability progression over 10 years later (after 1 and 2 years, respectively) [92]. Similarly, a large multicenter study showed that a combination of central atrophy rate and the lesion volume change over the first 2 years was able to predict the disability over 10 years (74.3% of explained variance in clinical outcome) [93]. The atrophy of the deep gray matter (especially the thalamus) has been repeatedly shown as an effective MRI measure that is able to predict future conversion of CIS patients to clinically defined MS or predict patients with future disability progression [94, 95]. There is an increasing amount of evidence that the GM and deep GM atrophy occurs more rapidly through all stages of the disease when compared to the WM and may present as a meaningful indicator of neurodegeneration [96, 97]. The ability to detect an early brain atrophy rate that will subsequently predict the long-term disability outcomes allows better therapy monitoring (Figs. 6.5 and 6.6) [98].

A meta-analysis from all published RRMS clinical trials showed close relationship between the treatment effect on brain atrophy and on disability progression [99]. The treatment effect demonstrated an independent effect on active MRI lesions, an independent effect on the brain atrophy, and a synergistic effect of both MRI outcomes combined [99]. Based on several long-term follow-up studies, cutoff values of pathological yearly brain atrophy have been purposed [100–102]. A combined analysis of multiple observational and interventional MS trials that included more than 11,000 MRI scans demonstrated that −0.57% annualized percentage change of corpus callosum volume had 90% specificity and 48% sensitivity in distinguishing between healthy controls and RRMS patients [101]. A small single-center study showed that an annual whole brain atrophy rate greater than 0.5% has 95% specificity or greater than 0.4% has 80% specificity in discriminating patients with MS from healthy controls [100]. Based on

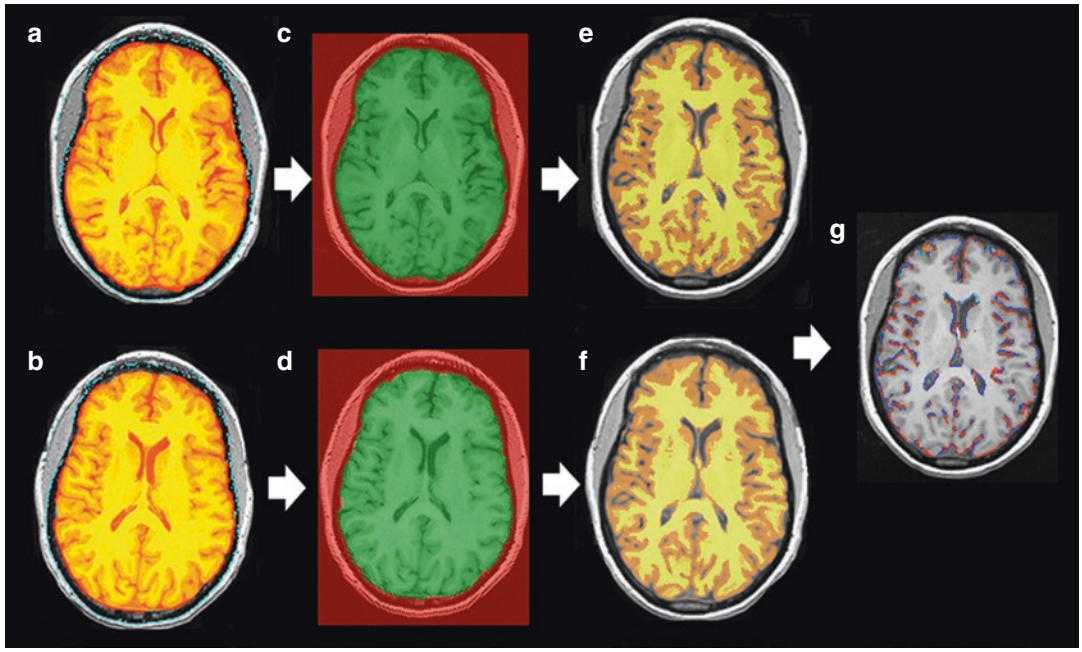

Fig. 6.5 Brain atrophy analysis using SIENA algorithm. SIENA algorithm for estimating the longitudinal total brain volume change between two input images taken from the same subject, at different timepoints. The upper row of images belongs to the initial MRI timepoint and the lower row of images belongs to the follow-up MRI timepoint. (**a**, **b**) Represent the extracted brain images, (**c**, **d**) demonstrate the standard space masking within a common field of view, while (**e**, **f**) show the tissue segmentation that detects the brain/non-brain boundaries. In panel **g**, the final brain edge movement image shows atrophy (blue) or "growth" (orange)

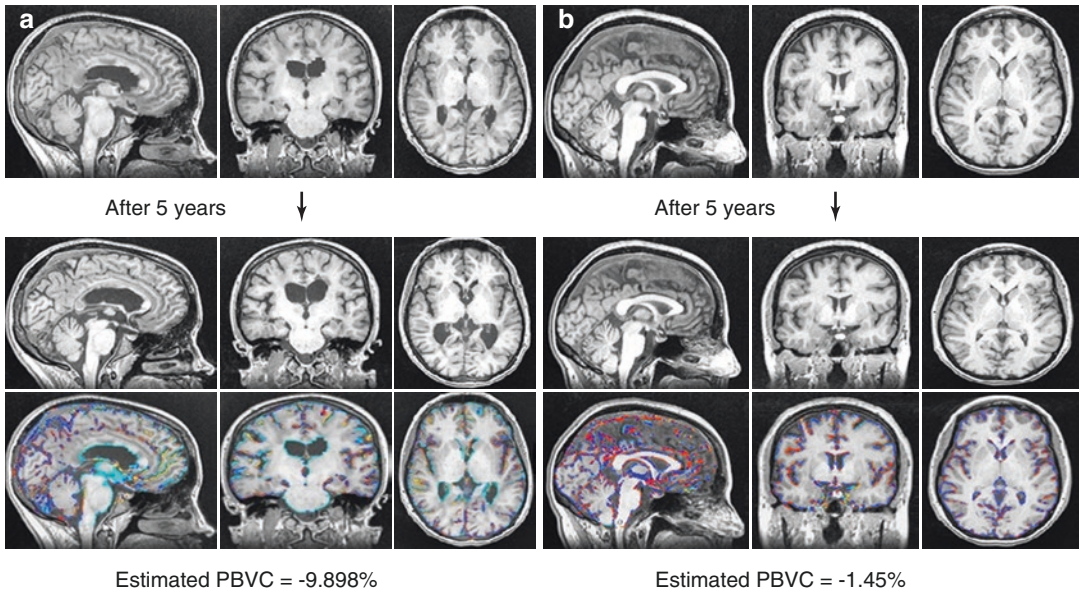

Fig. 6.6 Brain atrophy differences between age- and sex-matched relapsing–remitting multiple sclerosis patients assessed with SIENA alghoritm over a 5-year follow-up period. *PBVC* percentage brain volume change. The relapsing–remitting multiple sclerosis (RRMS) patient in panel (**a**) demonstrates a high rate of 5-year longitudinal atrophy rate (estimated PBVC = −9.898% or 1.98% annualized), whereas the age- and sex-matched RRMS patient in panel (**b**) demonstrates comparatively lower brain atrophy rate (estimated PBVC = −1.45% or 0.29% annualized)

the corresponding 0.4% of annual whole brain atrophy, similar sensitivity and specificity analysis determined the lateral ventricular volume cutoff at annual rate of 3.5% [102]. With a proposed individual expected brain volume calculation, the FREEDOMS I/FREEDOMS II trial patients were classified as low baseline volume (1 standard deviation below the expected), medium baseline brain volume (within 1 standard deviation of the expected), and high brain volume (1 standard deviation above the expected) [103]. Additional factors that were accounted into the model included the baseline age, sex, the disease duration, T2 lesion load and their baseline disability [103]. The aforementioned attempt of individual brain volume classification was able to differentiate patients with high risk of future disability worsening (low vs. high BV with hazard ratio of 1.73) [103]. Before undertaking the task of individual volumetric comparisons, it is critical to understand the processes of biological aging and the ability to separate the "normal aging atrophy" with "disease-specific atrophy" [104]. A step toward determining ideal regions that undergo disease-specific atrophy would ultimately lead to the ability of measuring the therapeutic interventions that would target the brain atrophy. Furthermore, the creation of a large population-wide volumetric database that archives the MRI scans and provides MS-specific atrophy rates across the lifespan of the patients may further overcome the current limitations of atrophy use [105]. Furthermore, the measurement of brain atrophy has special interest in the management of the questionably distinct and small cohort of patients (10%) termed as PPMS, which demonstrates continuous disability worsening despite the absence of clearly recognizable clinical relapses and active inflammatory MRI biomarkers [106].

The use and reliability of brain atrophy measurements in MS patients have substantially improved in the last two decades. Fully automated software like NeuroQuant®, MSmetrix™, and NeuroSTREAM® have been developed for computing cross-sectional and/or longitudinal changes of the whole brain volume, separate tissue-compartment volumes (GM and WM), and lateral ventricular CSF volumes, respectively [107]. Based on the characteristics of the MRI sequences that are currently acquired throughout the United States (99.3% availability of T2-FLAIR vs. only 39.7% of 3D T1-WI), developing a feasible surrogate T2-FLAIR-derived atrophy calculation may additionally assist in future implementation of atrophy outcomes [108]. Although brain atrophy now is regularly used as a secondary endpoint in all recent and upcoming MS clinical trials, the utility and interpretation of individual brain volume changes within the clinical routine remain undetermined [109].

Magnetization Transfer Imaging (MTI)

Magnetization transfer imaging (MTI) uses the different T_2 relaxation properties of water molecules that are found in a free state (>10 ms) or as bound to complex macromolecules (<200 μs). Application of an off-resonance RF pulse that will selectively pre-saturate only the immobile water protons causes exchange (transfer) of longitudinal magnetization between the rigid macromolecules and the free water protons. This magnetization transfer results in partial saturation of the free water molecules as well (it decreases the signal) and creates tissue contrast. The magnetization transfer ratio (MTR) can be quantified by acquiring and subtracting two sets of acquisitions, image with the off-resonance pulse (M_{sat}) and conventional image (M_0) (Fig. 6.7):

$$\mathrm{MTR} = \frac{M_0 - M_{sat}}{M_{sat}}$$

Decrease in MTR has been associated with loss of myelin, axonal damage, and active cell infiltration, whereas the increase of MTR has been hypothesized as marker of possible remyelination and lesion resolution [110, 111]. The use of this technique in understanding the MS pathology has been further standardized and implemented in several pivotal MS trials. In the DEFINE trial, a double-blind, placebo-controlled

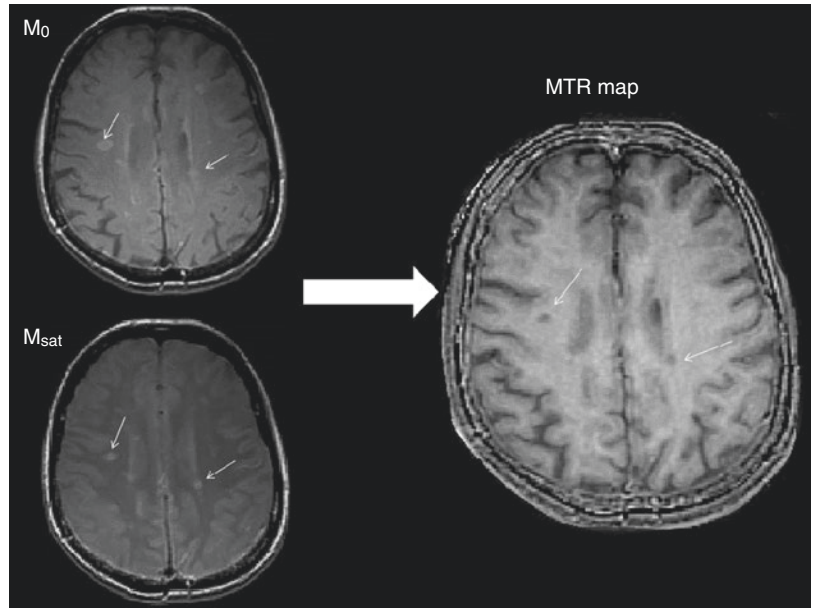

Fig. 6.7 Magnetization transfer imaging (MTI) in multiple sclerosis. The magnetization transfer ratio (MTR) obtained by subtracting two sets of acquisitions: image with the off-resonance pulse (M_{sat}) and conventional image (M_0). The decrease in MTR as represented by hypointense signal areas in the MTR map (white arrows) is associated with loss of myelin, axonal damage, and active cell infiltration

study that randomized patients to dimethyl fumarate and placebo, the active treatment showed significant normal-appearing brain tissue (NABT) reduction when compared to placebo [112]. The similar utility of longitudinal MTR imaging was seen in BECOME [113] and ADVANCE trials [114], demonstrating the MTR responsiveness in clinical intervention settings. The use of MTR imaging in future remyelination trials is also planned.

Average NABT MTR changes have shown good specificity and positive predictive value in predicting individual disability progression over the 4.5-year follow-up period [115]. Similarly, a combination of percentage change of lesion MTR and GM MTR values are able to discriminate 66% of the MS patients with risk of long-term disability progression [116]. These MTR changes are present even at the earliest stages of MS and are not correlated to the inflammatory burden of the patient, alluding to independent pathophysiology [117]. Independently of the lesion load, a similar study also showed that the periventricular MTR changes in CIS patients are associated with later definitive MS diagnosis and subsequent disability accumulation [118].

Consecutive MTR scans have demonstrated that progressive local decrease in MTR values in the NAWM precedes the development of enhancing lesions [119]. These changes appear 3 months before the Gd enhancement and may be attributed to perivascular inflammation, edema, astrocytic proliferation, and sequential demyelination [120]. At the time of enhancement the lesion shows major decrease of MTR that partially recovers over the following 4 months [121]. The heterogeneity is demonstrated where some lesions show partial recovery of the mean MTR, some show stable low levels of MTR, and others further continue to decline [121]. In situ, postmortem MTR imaging of seven MS brains showed that normalized MTR of the cortex was significantly lower in presence of cortical lesions when compared to myelinated cortex [122]. The imaging was performed on 3 T clinically available MTR sequences and may be of additional benefit in the detection of cortical lesions [122].

Overall, the MTI can be used as proxy measurement of the absolute myelin content and provides additional information on the overall pathophysiology of the processes seen in NABT and in MS lesion evolution. The availability of MTI in most of the modern MRI scanners allows obtainable and achievable MTI imaging in large clinical remyelination trials [123]. Myelin water imaging (MWI), quantitative magnetization

transfer (QMT), multi-echo T_2 mapping, and steady-state multicomponent relaxometry (mcDESPOT) are newer techniques that may further provide understanding of the myelin pathology observed in MS.

Multi-echo Imaging

Magnetic susceptibility is the physical quantity that measures the extent to which a material is magnetized when placed in an extrinsic magnetic field. This is an intrinsic property of all biological tissues and the brain susceptibility is mainly driven by four molecules: water, iron, myelin, and calcium [124]. The magnetic susceptibility causes local field perturbation that creates various distortions of the MRI images. Although these image distortions were initially considered as unwanted, a number of sequences take advantage of them as a useful image contrast [125]. In contrast to the nuclear magnetization of the MRI signal, magnetic susceptibility originates from the orbital electrons [126]. Multi-echo spoiled-gradient-recalled-echo (SPGR or GRE) sequence is the most common method of capturing the effect of the aforementioned magnetic susceptibility. The exponential decay (T_2* decay) measures the offset of the local Larmor frequency and captures the local field perturbations. Therefore, different biological tissues would have different T_2* values that allow early and quantitative diagnosis of diseases.

The simple MRI signal is an oscillating sinusoidal wave that has fundamental properties of frequency, amplitude, and phase. The susceptibility-weighed imaging (SWI) uses a combination of magnitude and phase in order to enhance the T_2* contrast derived from the magnetic field perturbations. The sensitivity of the conventional sequences to detect MS lesions is high; however, the lack of specificity can be potentially overcome by SWI. The initial use of MR venography showed that 94 out of 95 lesions seen in MS patients have a vein running centrally through them, demonstrating the perivenular distribution of the pathology [127]. The North American Imaging in Multiple Sclerosis (NAIMS) Cooperative later has recognized the utility of the "central vein sign" (CVS) as proposed MRI biomarker to increase the accuracy of the MS diagnosis [80]. Although the CVS can been seen among T2 hyperintensities originating from other inflammatory and non-inflammatory pathology, a threshold of 50% perivenular lesions allows MS discrimination with diagnostic accuracy of 100% [128]. Similar phase abnormalities are able to distinguish WM signal abnormalities in CIS patients and tend to be more predictive of conversion to definite MS than the conventional T2 lesions [129]. Outside of lesion discrimination, the SWI technique can be used in determining cerebral microbleeds [130] and abnormal phase tissue in the subcortical gray matter [131].

The field variations based on the biological magnetic susceptibility can be quantitatively assessed by quantitative susceptibility mapping (QSM) or susceptibility tensor imaging (STI) (Fig. 6.8). The potential use of QSM in MS imaging can be essential in understanding the substantial and long-lasting microglial inflammation that is actively occurring behind an intact BBB [132]. As such, changes in iron accumulation within the macrophages and microglia may provide additional information of the lesion evolution [133]. During active Gd enhancement, the susceptibility is initially isointense. As soon as the enhancement diminishes, the susceptibility drastically increases and remains constant until completely returning to the original isointense levels (formation of chronic silent lesions after several years) [134]. Similar use of QSM would allow detecting chronically active versus chronically inactive lesions. Lesions rich with iron-laden M1 microglia express proinflammatory cytokines that promote slow smothering tissue damage around the rim of the lesion [135].

Several cross-sectional and longitudinal MS studies showed heterogeneity in the iron trajectories of the deep GM. Accumulating evidence is demonstrating that certain structures like the caudate are progressively accumulating more iron, whereas the thalamus, pulvinar, and the left lateral nuclear region decrease their iron content [136]. The susceptibility reduction seen in the thalamus and the pulvinar is also associated with

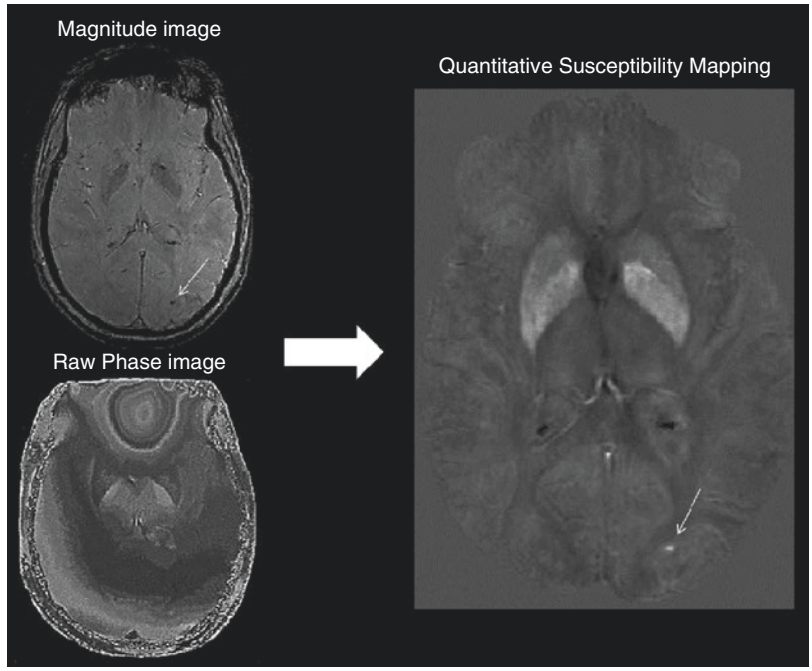

Fig. 6.8 Multi-echo phase imaging and quantitative susceptibility mapping (QSM) processing. Quantitative susceptibility mapping provides sensitive tool for assessing the amount of iron and calcium within the tissues. After a series of processing steps, the final image is derived from a magnitude and raw phase image. The white arrow points to a microbleed

longer disease duration [137]. The thalamic reduction of susceptibility may potentially suggest an active process of iron depletion within the oligodendrocytes [137].

Future QSM studies have the potential to understand the role of global iron trafficking in terms of lesion evolution and neurodegeneration. Additional T_2*-weighted methods that use the contrast from the magnetic field perturbations are myelin water imaging (MWI), STI, arterial spin labeling (ASL), and functional magnetic resonance imaging (fMRI).

Diffusion-Weighted Imaging (DWI) and Diffusion Tensor Imaging (DTI)

The diffusion measurement captures the random thermal (Brownian) motion of water molecules constrained by the surrounding anatomy. Therefore, diffusion-weighted imaging (DWI) provides information dominated mainly by static neuroanatomy and less influenced by the physiology of the system [138]. Diffusion of the water in a circular fashion (spreading toward all sides) is called *isotropic* diffusion, whereas water that diffuses along one specific axis is called *anisotropic* diffusion [139]. Diffusion tensor imaging (DTI) uses multiple DWI images acquired with different diffusion gradients that can be fitted into one diffusion tensor model and provides numerical quantification of mean diffusivity (MD), radial diffusivity (RD), axial diffusivity (AD), and fractional anisotropy (FA). Since water can easily diffuse along the length of the axonal bundles and between the myelin sheaths, the anisotropic properties allow estimation of axonal integrity and organization.

This technique has allowed systematic mapping of the macroscopic human brain circuits within projects like the Human Connectome Project (HCP), The BRAIN initiative, the Human Brain Project, and has a significant utility in understanding the MS pathology [140]. As mentioned previously, the disease hallmarks of axonal demyelination and neurodegeneration alter the geometry of the brain tissue and allow increase in isotropic diffusion. Preclinical models that are specific to demyelination and remyelination processes (cuprizone-induced mice models) demonstrated that the loss of myelin is a sufficient and independent driver of the RD change [141]. Although RD has been proposed as in vivo marker for demyelination, a multicompo-

nent analysis of additional DTI scalar maps substantially increases the accuracy in prediction of the lesion microstructure [142]. Similar to the previous MTI and QSM studies, DWI imaging can also detect local NAWM changes that occur 6 weeks before the enhancement appearance [143]. These DTI-derived changes continue to increase even after the enhancement subsides. Eventually, nine weeks after the enhancment, these lesions reach similar values to the ones of chronic MS lesion [143]. In comparison to WM lesions that are characterized with reduced FA, several studies have shown that the cortical lesions differ and demonstrate increase in their FA [144]. Compared to healthy controls, the increase in FA was also noted within the lesion-free GM [144]. This FA change in the GM can also help in explaining the long-term clinical outcomes in PPMS, a disease subtype that is still not fully characterized [145]. The contrasting results may be explained by the lower level of inflammation and the considerable increase in microglial proliferation seen in cortical lesions.

The DTI alterations are not only present in areas of current and/or future inflammatory involvement, but they are also widespread within the NABT and subcortical deep gray matter [146]. The DTI technique allows insight of the cerebral microscopic changes and provides deeper understanding of the structural changes that are otherwise not seen by conventional imaging [147]. For example, even when the volumetric changes are accounted for, the MD of the thalamus provides additional 7–13% of explained variance seen in the MS-associated cognitive decline [148]. Similarly, MS patients with slowing of their information processing speed showed reduction of FA within the corpus callosum, a region that is not primarily affected by T2-weighted lesions [149]. Since the corpus callosum is a vital structure for bi-hemispheric communication, any disruption of the callosal microstructural integrity may play an important role in the cognitive performance.

Future methods that should improve the in vivo evaluation of the structural integrity include tract-based spatial statistics (TBBS), diffusion kurtosis imaging (DKI), and neurite orientation dispersion and density imaging (NODDI). Diffusion-weighed imaging can advance the understanding of the structural changes that contribute toward cognition, fatigue, brain reserve, and plasticity. Longitudinal studies have showed DTI applicability in examining the temporal evolution of the structural integrity changes [150]. Although the use of pre-standardized protocols improves the feasibility of longitudinal assessments, there are still considerable differences attributed to the acquisition centers [151]. Before implementation of diffusion-based imaging into clinical trials, additional standardization is needed.

Functional Magnetic Resonance Imaging (fMRI)

The complex interplay between acute and chronic structural damage and the dynamic ability of the brain to adapt and recover is highlighting MS as ideal model for studying brain reserve and plasticity [152]. In general terms, processes in the brain activity changes are divided into adaptive (brain activity that will result in lowering the symptomatology) and maladaptive (brain activity that potentiates and worsens the existing symptomatology). This ability of structural, functional, and connection-wise reorganization can be measured and quantified using various MRI techniques. One accepted method of studying the change in activity is fMRI (Fig. 6.9). fMRI is an indirect measure of neuronal activity by measuring the amount of increased recruitment of oxygenated blood within the local cerebral blood flow. The hemodynamic response increases the delivery of oxygen-rich blood and displaces the deoxygenated one. Since deoxygenated hemoglobin has more magnetic properties (paramagnetic) when compared to the oxygenated hemoglobin, it produces changes in the magnetic field (T2∗) and creates MRI signal called blood-oxygen-level-dependent (BOLD) contrast.

Task-based fMRI (tb-fMRI) is used to identify brain regions that are activated during performing a specific task. Most motor tb-fMRI studies involve a task of finger tapping, whereas N-back

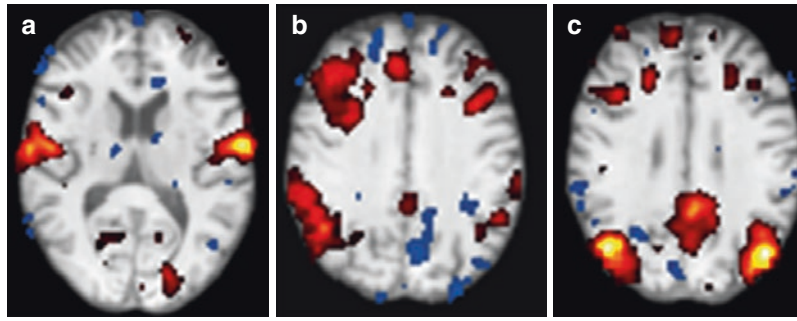

Fig. 6.9 Functional magnetic resonance imaging (fMRI) analysis. Independent component analysis of a single subjects resting-state fMRI time series reflects known functional networks. Panel (**a**) demonstrate's the sensory-motor network, (**b**) demonstrates the frontoparietal network, and (**c**) demonstrates default mode network

tasks are used to study brain regions activated during cognitive/memory performance. A classic example of an adaptive process that involves an active cortical area reorganization is the activation of contralateral motor area during an MS relapse [153]. Since the new lesion would interfere with pathways that were previously in use, the movement of the affected extremity results in activation of both the contralateral and in relative activation increase of the ipsilateral motor cortex [153]. Additionally, patients with established RRMS phenotype and no disability have increased supplementary motor area activation when compared to CIS patients [154]. This supplementary motor area activation might be due to additional recruitment of preexisting motor pathways and reflects the increased efforts in order to perform the same motor task [154]. More comprehensive reviews on the changes in connectivity associated with motor performance have been published [155].

In comparison to the traditional tb-fMRI, capturing the spontaneous BOLD signal alterations in absence of a stimulus or a task is called resting-state fMRI (rs-fMRI). The large rs-fMRI data can be analyzed by two main models: functional segregation and functional integration [156]. The former allows determination of brain regions according to their specific function. Among commonly used methods for functional segregation analysis are the regional homogeneity (ReHo) and amplitude of low frequency fluctuations (ALFF). The increasing recognition of the brain as complex integrated network rather than isolated activating regions has decreased the use of the functional segregation methods as preferred rs-fMRI analysis. On the other hand, the functional integration analysis allows measurement of the BOLD synchrony between two different brain regions. This synchrony does not imply structural connection of the regions (DTI-derived information) but the synchronic connectivity can be a result through an indirect link or mediating regions. Methods for functional integration analysis include independent component analysis (ICA) [157], ROI-based functional connectivity analysis [158], and graph analysis [159]. The default mode network (DMN) has been the most commonly studied network in the rs-fMRI analysis. This network is highly active during rest and decreases in activity over a broad range of goal-orientated cognitive tasks and is therefore named "task-negative" network [160]. The lack of DMN reduction during task performance results in decrease in attention and lower cognitive performance in healthy individuals [161]. The activity of DMN has been also negatively correlated with other task-based networks like the attention network [162].

In the early stages of MS, the diverging role of anatomical and functional connectivity measurements has been shown [163]. As the anatomical connectivity declines (a lesion causing disconnection between regions), the functional connectivity shows concurrent and compensatory increase in activity. However, in the later stages of the disease, the ability to activate larger brain regions gets depleted and an overall

decrease in activity is noted [164]. This decrease also has been associated with the T2 lesions load and correlated with disability [164]. Similarly, during the execution of the N-back task, the fMRI analysis demonstrated that cognitively impaired MS patients have decreased activity in the frontal regions and increased activity of the DMN network [165]. The aforementioned graph theory allows formation of networks that are defined by multiple nodes that are functionally connected. Parameters like modularity, centrality, clustering coefficient, and node degree describe this "small-world" network as organization that attempts to deliver information by spending the lowest energy in the most effective way possible [166]. This method was applied on 246 MS patients and 55 matched healthy controls and showed that MS patients had loss of network hubs, right lateralization of the basal ganglia, and formation of new hubs in the temporal lobe and cerebellum [167]. The impaired network was not able to exchange information efficiently and the analysis was able to discriminate the cognitively impaired patients [167].

The previous analysis of functional connectivity solemnly depends on correlation between two remote brain regions and does not provide dynamic information. On the other hand, effective connectivity allows making inferences on the effect that one neuronal system exerts over another region, both on a synaptic or population based level [168]. Since there is no single method that defines the brain connectivity on its own, use of multiple complementary analyses may yield more complete connectivity characterization. The use of fMRI would substantially help in understanding the physiological background of cognitive decline, fatigue, and brain plasticity seen in MS patients [169].

Magnetic Resonance Spectroscopy (MRS)

^{1}H-Magnetic Resonance Spectroscopy (^{1}H-MRS) allows imaging and quantifying the number of hydrogen protons that are positioned within different shielding environments. Since the number of hydrogen protons situated within the molecules of water and fat is several thousand times higher than the amount of hydrogen protons within other molecules, an active water suppression is essential in visualizing the lower spectral peaks. This is usually performed with narrow bandwidth frequency-selective pulse (Chemical Shift Selective or CHESS), which is applied exactly at the Larmor frequency of the water. Recording of the free induction decay allows peaks to be plotted on a line that usually starts with 0 ppm molecule (tetra-methyl silane) at the left and until the suppressed water peak at 4.7 ppm at the right of the spectrum (Fig. 6.10). Since the ability to separate the peaks (spectral dispersion) is directly proportional to B_0, ultra-high-field MRS imaging enables enhanced capability of metabolite detection.

N-acetylaspartate (NAA), *myo*-inositol (mI), choline (Cho), creatine (Cr), glutamate (Glu), gamma-aminobutyric acid (GABA), and lactate (Lac) are several brain metabolites that are of particular interest in MS pathology [170]. After glutamate, NAA is the second most prevalent brain metabolite and colocalizes in the neuronal bodies, proximal dendrites, and axons [171]. Therefore, quantification of the NAA peak would generally provide valuable information about the neuronal integrity and neurodegeneration. Recent studies also showed high levels of NAA within the myelin itself [172]. The concentrations of NAA in the myelin of the WM tracts were comparable, or higher, to the cytosol of the central axon [172]. On the contrary, mI is a metabolite not seen in neurons but appears to be specific to the glia cells [173]. Due to its sugar-like properties, mI functions as the brain osmolyte, thus controlling the cell volume and fluid distribution. Additionally, mI is an essential precursor for the phospholipid molecules that are found in phospholipid cell membranes and myelin sheaths. Cho reflects the overall cell-membrane turnover, and elevated concentrations are seen in active processes of demyelination, remyelination, gliosis, and inflammation [174]. Lactate metabolite is an end product of the less efficient anaerobic glycolysis. As this metabolite is usually not present in a healthy brain tissue, it might define areas of

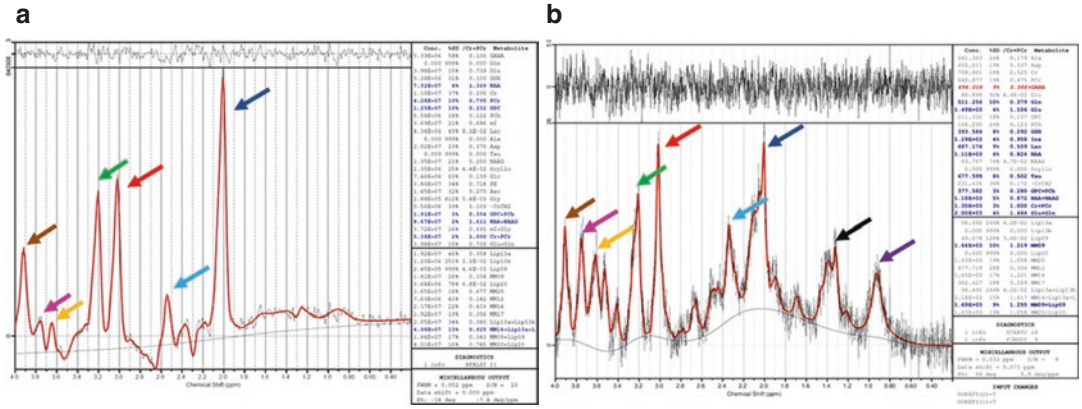

Fig. 6.10 Magnetic resonance spectroscopy (MRS) frequency spectrum from human and mouse thalamus imaged on 3 T Toshiba MRI and on 9.4 T Bruker MRI scanners, respectively. Panel (**a**) demonstrates magnetic resonance spectroscopy (MRS) output form healthy human thalamus imaged with point resolved spectroscopy (PRESS) sequence on a 3 T Canon Medical MRI. Similarly, the panel (**b**) demonstrates the same PRESS sequence utilized for imaging of mouse thalamus on a 9.4 T Bruker MRI scanner. The major MRS metabolite peaks are shown in increasing particles per million (from right to left) and labeled with different arrows: dark blue—*N*-acetyl aspartate, cyan—glutamate, glutamine, and GABA, red and pink—creatine and phosphocreatine, green—choline, yellow—*myo*-inositol and brown—glucose. The higher magnetic field (B_0) of 9.4 T scanner allows better separation of the aforementioned metabolic peaks and isolation of additional peaks like lipids (magenta) and lactate (black). All peaks and their absolute quantification are shown in the corresponding MRS output

mitochondrial dysfunction and/or increased energy consumption [175]. Finally, Cr levels have been associated with the extent of gliosis.

As the pathology of the MS brain is not strictly confined to the T2-hyperintense lesions, the MRS imaging (similarly to the MTI) has also focused on two separate regions: lesions and the NABT.

The use of ^{1}H-MRS in lesion analysis is heavily limited by the spatial resolution of the technique. Due to the large size of the MRS voxel, partial volumes from the NAWM and CSF space will contaminate the lesional output. Therefore, most of early MS spectroscopy analyses were confined to lesions larger than 1 cm^3, despite the fact that these lesions are not characteristic of the disease itself. Several studies have examined the metabolic changes through the evolution of the lesions [176–178]. The concentrations of mI, Cr, and Cho in the pre-lesional tissue were not different when compared to chronic lesions, whereas the levels of NAA were higher [176]. This finding demonstrates that the processes responsible for lesion formation can be detected even before the actual lesion formation [176]. The additional drop of the NAA levels coincides with the appearance of the acute lesion on conventional T2-WI. In months following the lesion appearance, the maintenance of low NAA levels was associated with persistence of the T2-hyperintensity, whereas NAA recovery was correlated with concurrent resolution of the lesion [176].

The decrease in NAA/Cr ratio is among the most reproducible changes within the NABT of MS patients [179, 180]. The changes within the NABT are seen both in relation to the vicinity of coexisting MS lesions, implying axonal transection, and in their complete absence [18, 181]. In testimony of the aforementioned diffuse brain pathology, a PPMS study demonstrated substantial decrease of the NAA/Cr ratio within the NABT and showed no differences when compared to the NAA levels measured at T2 lesions [182]. Similarly, a direct quantitative metabolite comparison showed no difference between the chronic T2 lesions and the NAWM [183]. The elevated markers of glial proliferation but normal levels of axonal injury during clinical remission are suggestive of ongoing diffuse inflammation that precedes the structural damage and brain atrophy [184]. A longitudinal ^{1}H-MRS study showed that the

higher baseline ratio of mI:NAA measured in the NAWM can be considered as predictive of future brain atrophy [185]. This biomarker was also able to predict future changes in the EDSS, MS Functional Composite (MSFC), and in prediction of 12-month sustained EDSS progression [185]. The combined examination of several metabolites better portrays the complex pathophysiology of neuronal loss, gliosis, and inflammation. Future advances into the field of MRS imaging should include use of high field MRI strengths, diffusion-weighted spectroscopy (DW-MRS), improvement in the absolute quantification of the metabolites, and use of other MRS atomic nuclei like phosphorus (^{31}P), carbon (^{13}C), and fluorine (^{19}F).

Additionally by using ^{1}H-Nuclear Magnetic Resonance (^{1}H-NMR) spectroscopy, collected blood or CSF samples from MS patients can be ex vivo analyzed. For example, blood-derived samples showed metabolic differences within the tryptophan and energy metabolism [186]. The aforementioned pathways have been previously associated with MS pathology [187].

Quantitative and Synthetic MRI (qMRI/syMRI)

Quantitative MRI (qMRI) uses the principal physical properties that create the MRI image: longitudinal relaxation rate (R_1), transverse relaxation rate (R_2), and the proton density (PD). Biological processes like inflammation, axonal injury, and gliosis will directly influence the relaxation properties of the tissue and cause absolute changes in R_1, R_2, and PD values. Absolute quantification of the relaxation times will allow direct comparison of a single patient to a referenced and matched healthy group. As an additional benefit, the large sample size of acquired quantitative maps can be used for creating common brain templates and allow automated brain region segmentation. The qMRI method has been shown to outperform the conventional MRI imaging in detection of both WM and cortical lesions [188]. Similarly, qMRI measurements of the NABT show strong correlations with measures of clinical disability and may further allow in vivo analysis of the MS pathophysiology [189].

Although the principles of absolute measurement of T1 and T2 relaxation times were initially described 60 years ago, the long scanning time and the high background noise has limited its clinical use [190]. Recent development of fast quantitative protocols like "quantification of relaxation times and proton density by multiecho acquisition of a saturation-recovery using turbo spin-echo readout (QRAPMASTER)" allows automated lesion segmentation, brain volume quantification, and mapping of the myelin based on the quantitative analysis [191]. Synthesis of the scans (syMRI) are based on the absolute quantitative values and allow complete head coverage within scan time of 6 min [192]. This short scanning time of syMRI produces good quality images that can be of great benefit to the pediatric population and the critically ill patients [192]. Additionally, the syMRI uses the acquired inverse relaxation time values (R_1, R_2, and PD) to create virtual signal intensities in any combination of an echo and repetition time. Since most clinical radiologist have limited experience in reading quantitative maps, the syMRI also allows creation of T1-WI, T2-WI, and PD-WI that resemble the conventionally weighted contrast images. Currently, the synthetic MRI protocols are in the process of regulatory approval in several countries and will be integrated into the platforms provided by GE, Philips, and Siemens.

Conclusion

MRI remains the most sensitive diagnostic and prognostic biomarker for MS patients. The current conventional MRI techniques have been additionally optimized for better detection of active and chronic lesions. However, the recent findings of widespread activity within the NABT have limited their use in fully apprehending the pathophysiology of MS. The nonconventional MRI techniques, new cell-specific contrast agents, synthetic MRI, and ultra-high-field scanners are among many MRI advancements that are

able to provide better understanding of the underlying disease pathology. Use of nonconventional techniques in the development of new clinical trials would additionally help to identify patients that would most benefit from the examined medication. Similarly, implementation of modalities that provide microstructural and myelin information can help with the discovery of future protective and remyelination medications. Before clinical implementation of these modalities, further standardization is still warranted.

Acknowledgments We are grateful to Dr. Ferdinand Schweser (University at Buffalo, BNAC) and Tom Fuchs (University at Buffalo, BNAC) for providing the magnetic resonance spectroscopy (MRS) and functional magnetic resonance imaging (fMRI) figures, respectively.

References

1. Reich DS, Lucchinetti CF, Calabresi PA. Multiple sclerosis. N Engl J Med. 2018;378(2):169–80.
2. Brownlee WJ, Hardy TA, Fazekas F, Miller DH. Diagnosis of multiple sclerosis: progress and challenges. Lancet. 2017;389(10076):1336–46.
3. Cree B, Gourraud PA, Oksenberg JR, Bevan C, Crabtree-Hartman E, Gelfand JM, et al. Long-term evolution of multiple sclerosis disability in the treatment era. Ann Neurol. 2016;80(4):499–510.
4. Zivadinov R, Leist TP. Clinical-magnetic resonance imaging correlations in multiple sclerosis. J Neuroimaging. 2005;15(4 Suppl):10S–21S.
5. Barkhof F. The clinico-radiological paradox in multiple sclerosis revisited. Curr Opin Neurol. 2002;15(3):239–45.
6. Healy BC, Buckle GJ, Ali EN, Egorova S, Khalid F, Tauhid S, et al. Characterizing clinical and MRI dissociation in patients with multiple sclerosis. J Neuroimaging. 2017;27(5):481–5.
7. Poloni G, Minagar A, Haacke EM, Zivadinov R. Recent developments in imaging of multiple sclerosis. Neurologist. 2011;17(4):185–204.
8. Zivadinov R, Bakshi R. Role of MRI in multiple sclerosis I: inflammation and lesions. Front Biosci. 2004;9:665–83.
9. Gawne-Cain ML, O'Riordan JI, Thompson AJ, Moseley IF, Miller DH. Multiple sclerosis lesion detection in the brain: a comparison of fast fluid-attenuated inversion recovery and conventional T2-weighted dual spin echo. Neurology. 1997;49(2):364–70.
10. Tintore M, Rovira A, Rio J, Otero-Romero S, Arrambide G, Tur C, et al. Defining high, medium and low impact prognostic factors for developing multiple sclerosis. Brain. 2015;138(Pt 7):1863–74.
11. Jakimovski D, Kolb C, Ramanathan M, Zivadinov R, Weinstock-Guttman B. Interferon beta for multiple sclerosis. Cold Spring Harb Perspect Med. 2018;8(11):pii:a032003.
12. Fisniku LK, Brex PA, Altmann DR, Miszkiel KA, Benton CE, Lanyon R, et al. Disability and T2 MRI lesions: a 20-year follow-up of patients with relapse onset of multiple sclerosis. Brain. 2008;131(Pt 3):808–17.
13. Dolezal O, Dwyer MG, Horakova D, Havrdova E, Minagar A, Balachandran S, et al. Detection of cortical lesions is dependent on choice of slice thickness in patients with multiple sclerosis. Int Rev Neurobiol. 2007;79:475–89.
14. Tubridy N, Barker GJ, Macmanus DG, Moseley IF, Miller DH. Three-dimensional fast fluid attenuated inversion recovery (3D fast FLAIR): a new MRI sequence which increases the detectable cerebral lesion load in multiple sclerosis. Br J Radiol. 1998;71(848):840–5.
15. Bink A, Schmitt M, Gaa J, Mugler JP 3rd, Lanfermann H, Zanella FE. Detection of lesions in multiple sclerosis by 2D FLAIR and single-slab 3D FLAIR sequences at 3.0 T: initial results. Eur Radiol. 2006;16(5):1104–10.
16. Polak P, Magnano C, Zivadinov R, Poloni G. 3D FLAIRED: 3D fluid attenuated inversion recovery for enhanced detection of lesions in multiple sclerosis. Magn Reson Med. 2012;68(3):874–81.
17. Garcia-Lorenzo D, Francis S, Narayanan S, Arnold DL, Collins DL. Review of automatic segmentation methods of multiple sclerosis white matter lesions on conventional magnetic resonance imaging. Med Image Anal. 2013;17(1):1–18.
18. Trapp BD, Peterson J, Ransohoff RM, Rudick R, Mork S, Bo L. Axonal transection in the lesions of multiple sclerosis. N Engl J Med. 1998;338(5):278–85.
19. van Waesberghe JH, van Walderveen MA, Castelijns JA, Scheltens P, Lycklama a Nijeholt GJ, Polman CH, et al. Patterns of lesion development in multiple sclerosis: longitudinal observations with T1-weighted spin-echo and magnetization transfer MR. AJNR Am J Neuroradiol. 1998;19(4):675–83.
20. Bagnato F, Jeffries N, Richert ND, Stone RD, Ohayon JM, McFarland HF, et al. Evolution of T1 black holes in patients with multiple sclerosis imaged monthly for 4 years. Brain. 2003;126(Pt 8):1782–9.
21. Giorgio A, Stromillo ML, Bartolozzi ML, Rossi F, Battaglini M, De Leucio A, et al. Relevance of hypointense brain MRI lesions for long-term worsening of clinical disability in relapsing multiple sclerosis. Mult Scler. 2014;20(2):214–9.
22. Minneboo A, Uitdehaag BM, Jongen P, Vrenken H, Knol D, van Walderveen MA, et al. Association between MRI parameters and the MS severity scale: a 12 year follow-up study. Mult Scler. 2009;15(5):632–7.
23. Wattjes MP, Rovira A, Miller D, Yousry TA, Sormani MP, de Stefano MP, et al. Evidence-based guide-

lines: MAGNIMS consensus guidelines on the use of MRI in multiple sclerosis–establishing disease prognosis and monitoring patients. Nat Rev Neurol. 2015;11(10):597–606.
24. Rotstein DL, Healy BC, Malik MT, Chitnis T, Weiner HL. Evaluation of no evidence of disease activity in a 7-year longitudinal multiple sclerosis cohort. JAMA Neurol. 2015;72(2):152–8.
25. Silver NC, Tofts PS, Symms MR, Barker GJ, Thompson AJ, Miller DH. Quantitative contrast-enhanced magnetic resonance imaging to evaluate blood-brain barrier integrity in multiple sclerosis: a preliminary study. Mult Scler. 2001;7(2):75–82.
26. Mathews VP, Caldemeyer KS, Lowe MJ, Greenspan SL, Weber DM, Ulmer JL. Brain: gadolinium-enhanced fast fluid-attenuated inversion-recovery MR imaging. Radiology. 1999;211(1):257–63.
27. Absinta M, Vuolo L, Rao A, Nair G, Sati P, Cortese IC, et al. Gadolinium-based MRI characterization of leptomeningeal inflammation in multiple sclerosis. Neurology. 2015;85(1):18–28.
28. Zurawski J, Lassmann H, Bakshi R. Use of magnetic resonance imaging to visualize leptomeningeal inflammation in patients with multiple sclerosis: a review. JAMA Neurol. 2016;74(1):100–9.
29. Zivadinov R, Ramasamy DP, Vaneckova M, Gandhi S, Chandra A, Hagemeier J, et al. Leptomeningeal contrast enhancement is associated with progression of cortical atrophy in MS: a retrospective, pilot, observational longitudinal study. Mult Scler. 2017;23(10):1336–45.
30. Harrison DM, Wang KY, Fiol J, Naunton K, Royal W 3rd, Hua J, et al. Leptomeningeal enhancement at 7T in multiple sclerosis: frequency, morphology, and relationship to cortical volume. J Neuroimaging. 2017;27(5):461–8.
31. Jakimovski D, Weinstock-Guttman B, Ramanathan M, Kolb C, Hojnacki D, Minagar A, et al. Ocrelizumab: a B-cell depleting therapy for multiple sclerosis. Expert Opin Biol Ther. 2017;17(9):1163–72.
32. Zivadinov R, Pirko I. Advances in understanding gray matter pathology in multiple sclerosis: are we ready to redefine disease pathogenesis? BMC Neurol. 2012;12:9.
33. Wattjes MP, Lutterbey GG, Gieseke J, Träber F, Klotz L, Schmidt S, et al. Double inversion recovery brain imaging at 3T: diagnostic value in the detection of multiple sclerosis lesions. AJNR Am J Neuroradiol. 2007;28(1):54–9.
34. Eichinger P, Kirschke JS, Hoshi MM, Zimmer C, Muhlau M, Riederer I. Pre- and postcontrast 3D double inversion recovery sequence in multiple sclerosis: a simple and effective MR imaging protocol. AJNR Am J Neuroradiol. 2017;38(10):1941–5.
35. Eichinger P, Wiestler H, Zhang H, Biberacher V, Kirschke JS, Zimmer C, et al. A novel imaging technique for better detecting new lesions in multiple sclerosis. J Neurol. 2017;38(10):1941–5.
36. Seewann A, Kooi EJ, Roosendaal SD, Pouwels PJ, Wattjes MP, van der Valk P, et al. Postmortem verification of MS cortical lesion detection with 3D DIR. Neurology. 2012;78(5):302–8.
37. Geurts JJ, Roosendaal SD, Calabrese M, Ciccarelli O, Agosta F, Chard DT, et al. Consensus recommendations for MS cortical lesion scoring using double inversion recovery MRI. Neurology. 2011;76(5):418–24.
38. Calabrese M, Poretto V, Favaretto A, Alessio S, Bernardi V, Romualdi C, et al. Cortical lesion load associates with progression of disability in multiple sclerosis. Brain. 2012;135(Pt 10):2952–61.
39. Rovira A, Wattjes MP, Tintore M, Tur C, Yousry TA, Sormani MP, et al. Evidence-based guidelines: MAGNIMS consensus guidelines on the use of MRI in multiple sclerosis-clinical implementation in the diagnostic process. Nat Rev Neurol. 2015;11(8):471–82.
40. Korchinski DJ, Taha M, Yang R, Nathoo N, Dunn JF. Iron oxide as an MRI contrast agent for cell tracking. Magn Reson Insights. 2015;8(Suppl 1):15–29.
41. McAteer MA, Sibson NR, von zur Muhlen C, Schneider JE, Lowe AS, Warrick N, et al. In vivo magnetic resonance imaging of acute brain inflammation using microparticles of iron oxide. Nat Med. 2007;13:1253.
42. van Kasteren SI, Campbell SJ, Serres S, Anthony DC, Sibson NR, Davis BG. Glyconanoparticles allow pre-symptomatic in vivo imaging of brain disease. Proc Natl Acad Sci U S A. 2009;106(1):18–23.
43. Vellinga MM, Oude Engberink RD, Seewann A, Pouwels PJ, Wattjes MP, van der Pol SM, et al. Pluriformity of inflammation in multiple sclerosis shown by ultra-small iron oxide particle enhancement. Brain. 2008;131(Pt 3):800–7.
44. Oude Engberink RD, Blezer EL, Dijkstra CD, van der Pol SM, van der Toorn A, de Vries HE. Dynamics and fate of USPIO in the central nervous system in experimental autoimmune encephalomyelitis. NMR Biomed. 2010;23(9):1087–96.
45. Ramalho J, Ramalho M, Jay M, Burke LM, Semelka RC. Gadolinium toxicity and treatment. Magn Reson Imaging. 2016;34(10):1394–8.
46. Hao D, Ai T, Goerner F, Hu X, Runge VM, Tweedle M. MRI contrast agents: basic chemistry and safety. J Magn Reson Imaging. 2012;36(5):1060–71.
47. Kanda T, Ishii K, Kawaguchi H, Kitajima K, Takenaka D. High signal intensity in the dentate nucleus and globus pallidus on unenhanced T1-weighted MR images: relationship with increasing cumulative dose of a gadolinium-based contrast material. Radiology. 2014;270(3):834–41.
48. McDonald JS, McDonald RJ, Jentoft ME, Paolini MA, Murray DL, Kallmes DF, et al. Intracranial gadolinium deposition following gadodiamide-enhanced magnetic resonance imaging in pediatric patients: a case-control study. JAMA Pediatr. 2017;171(7):705–7.
49. Robert P, Lehericy S, Grand S, Violas X, Fretellier N, Idee JM, et al. T1-weighted hypersignal in the

deep cerebellar nuclei after repeated administrations of gadolinium-based contrast agents in healthy rats: difference between linear and macrocyclic agents. Investig Radiol. 2015;50(8):473–80.
50. Robert P, Violas X, Grand S, Lehericy S, Idee JM, Ballet S, et al. Linear gadolinium-based contrast agents are associated with brain gadolinium retention in healthy rats. Investig Radiol. 2016;51(2):73–82.
51. Gulani V, Calamante F, Shellock FG, Kanal E, Reeder SB, International Society for Magnetic Resonance in M. Gadolinium deposition in the brain: summary of evidence and recommendations. Lancet Neurol. 2017;16(7):564–70.
52. Polman CH, Reingold SC, Edan G, Filippi M, Hartung HP, Kappos L, et al. Diagnostic criteria for multiple sclerosis: 2005 revisions to the "McDonald Criteria". Ann Neurol. 2005;58(6):840–6.
53. Polman CH, Reingold SC, Banwell B, Clanet M, Cohen JA, Filippi M, et al. Diagnostic criteria for multiple sclerosis: 2010 revisions to the McDonald criteria. Ann Neurol. 2011;69(2):292–302.
54. Thompson AJ, Banwell BL, Barkhof F, Carroll WM, Coetzee T, Comi G, et al. Diagnosis of multiple sclerosis: 2017 revisions of the McDonald criteria. Lancet Neurol. 2018;17(2):162–73.
55. Huss AM, Halbgebauer S, Ockl P, Trebst C, Spreer A, Borisow N, et al. Importance of cerebrospinal fluid analysis in the era of McDonald 2010 criteria: a German-Austrian retrospective multicenter study in patients with a clinically isolated syndrome. J Neurol. 2016;263(12):2499–504.
56. Kuhle J, Disanto G, Dobson R, Adiutori R, Bianchi L, Topping J, et al. Conversion from clinically isolated syndrome to multiple sclerosis: a large multicentre study. Mult Scler. 2015;21(8):1013–24.
57. Dobson R, Ramagopalan S, Davis A, Giovannoni G. Cerebrospinal fluid oligoclonal bands in multiple sclerosis and clinically isolated syndromes: a meta-analysis of prevalence, prognosis and effect of latitude. J Neurol Neurosurg Psychiatry. 2013;84(8):909–14.
58. Filippi M, Preziosa P, Meani A, Ciccarelli O, Mesaros S, Rovira A, et al. Prediction of a multiple sclerosis diagnosis in patients with clinically isolated syndrome using the 2016 MAGNIMS and 2010 McDonald criteria: a retrospective study. Lancet Neurol. 2018;17(2):133–42.
59. Brownlee WJ, Swanton JK, Miszkiel KA, Miller DH, Ciccarelli O. Should the symptomatic region be included in dissemination in space in MRI criteria for MS? Neurology. 2016;87(7):680–3.
60. Filippi M, Rocca MA, Ciccarelli O, De Stefano N, Evangelou N, Kappos L, et al. MRI criteria for the diagnosis of multiple sclerosis: MAGNIMS consensus guidelines. Lancet Neurol. 2016;15(3):292–303.
61. Galetta SL, Balcer LJ. The optic nerve should be included as one of the typical CNS regions for establishing dissemination in space when diagnosing MS – YES. Mult Scler. 2018;24(2):121–2.
62. Kilsdonk ID, Jonkman LE, Klaver R, van Veluw SJ, Zwanenburg JJ, Kuijer JP, et al. Increased cortical grey matter lesion detection in multiple sclerosis with 7 T MRI: a post-mortem verification study. Brain. 2016;139(Pt 5):1472–81.
63. Maranzano J, Rudko DA, Arnold DL, Narayanan S. Manual segmentation of MS cortical lesions using MRI: a comparison of 3 MRI reading protocols. AJNR Am J Neuroradiol. 2016;37(9):1623–8.
64. Gabelic T, Ramasamy DP, Weinstock-Guttman B, Hagemeier J, Kennedy C, Melia R, et al. Prevalence of radiologically isolated syndrome and white matter signal abnormalities in healthy relatives of patients with multiple sclerosis. AJNR Am J Neuroradiol. 2014;35(1):106–12.
65. Keegan BM, Kaufmann TJ, Weinshenker BG, Kantarci OH, Schmalstieg WF, Paz Soldan MM, et al. Progressive solitary sclerosis: gradual motor impairment from a single CNS demyelinating lesion. Neurology. 2016;87(16):1713–9.
66. Spadaro M, Gerdes LA, Krumbholz M, Ertl-Wagner B, Thaler FS, Schuh E, et al. Autoantibodies to MOG in a distinct subgroup of adult multiple sclerosis. Neurol Neuroimmunol Neuroinflamm. 2016;3(5):e257.
67. Kearney H, Miller DH, Ciccarelli O. Spinal cord MRI in multiple sclerosis—diagnostic, prognostic and clinical value. Nat Rev Neurol. 2015;11(6):327–38.
68. Zalewski NL, Flanagan EP, Keegan BM. Evaluation of idiopathic transverse myelitis revealing specific myelopathy diagnoses. Neurology. 2018;90(2):e96–e102.
69. Arrambide G, Rovira A, Sastre-Garriga J, Tur C, Castillo J, Rio J, et al. Spinal cord lesions: a modest contributor to diagnosis in clinically isolated syndromes but a relevant prognostic factor. Mult Scler. 2018;24(3):301–12.
70. Brownlee WJ, Altmann DR, Alves Da Mota P, Swanton JK, Miszkiel KA, Wheeler-Kingshott CG, et al. Association of asymptomatic spinal cord lesions and atrophy with disability 5 years after a clinically isolated syndrome. Mult Scler. 2017;23(5):665–74.
71. Schlaeger R, Papinutto N, Panara V, Bevan C, Lobach IV, Bucci M, et al. Spinal cord gray matter atrophy correlates with multiple sclerosis disability. Ann Neurol. 2014;76(4):568–80.
72. Schlaeger R, Papinutto N, Zhu AH, Lobach IV, Bevan CJ, Bucci M, et al. Association between thoracic spinal cord gray matter atrophy and disability in multiple sclerosis. JAMA Neurol. 2015;72(8):897–904.
73. Zivadinov R, Banas AC, Yella V, Abdelrahman N, Weinstock-Guttman B, Dwyer MG. Comparison of three different methods for measurement of cervical cord atrophy in multiple sclerosis. AJNR Am J Neuroradiol. 2008;29(2):319–25.
74. Cawley N, Tur C, Prados F, Plantone D, Kearney H, Abdel-Aziz K, et al. Spinal cord atrophy as a primary

outcome measure in phase II trials of progressive multiple sclerosis. Mult Scler. 2018;24(7):932–41.
75. Martin AR, Aleksanderek I, Cohen-Adad J, Tarmohamed Z, Tetreault L, Smith N, et al. Translating state-of-the-art spinal cord MRI techniques to clinical use: a systematic review of clinical studies utilizing DTI, MT, MWF, MRS, and fMRI. Neuroimage Clin. 2016;10:192–238.
76. Filippi M, Evangelou N, Kangarlu A, Inglese M, Mainero C, Horsfield MA, et al. Ultra-high-field MR imaging in multiple sclerosis. J Neurol Neurosurg Psychiatry. 2014;85(1):60–6.
77. Mistry N, Tallantyre EC, Dixon JE, Galazis N, Jaspan T, Morgan PS, et al. Focal multiple sclerosis lesions abound in 'normal appearing white matter'. Mult Scler. 2011;17(11):1313–23.
78. Tallantyre EC, Dixon JE, Donaldson I, Owens T, Morgan PS, Morris PG, et al. Ultra-high-field imaging distinguishes MS lesions from asymptomatic white matter lesions. Neurology. 2011;76(6):534–9.
79. Gaitan MI, Sati P, Inati SJ, Reich DS. Initial investigation of the blood-brain barrier in MS lesions at 7 tesla. Mult Scler. 2013;19(8):1068–73.
80. Sati P, Oh J, Constable RT, Evangelou N, Guttmann CR, Henry RG, et al. The central vein sign and its clinical evaluation for the diagnosis of multiple sclerosis: a consensus statement from the North American Imaging in Multiple Sclerosis Cooperative. Nat Rev Neurol. 2016;12(12):714–22.
81. Pitt D, Boster A, Pei W, Wohleb E, Jasne A, Zachariah CR, et al. Imaging cortical lesions in multiple sclerosis with ultra-high-field magnetic resonance imaging. Arch Neurol. 2010;67(7):812–8.
82. Schmierer K, Parkes HG, So PW, An SF, Brandner S, Ordidge RJ, et al. High field (9.4 Tesla) magnetic resonance imaging of cortical grey matter lesions in multiple sclerosis. Brain. 2010;133(Pt 3):858–67.
83. Mainero C, Louapre C, Govindarajan ST, Gianni C, Nielsen AS, Cohen-Adad J, et al. A gradient in cortical pathology in multiple sclerosis by in vivo quantitative 7 T imaging. Brain. 2015;138(Pt 4):932–45.
84. Scalfari A, Neuhaus A, Degenhardt A, Rice GP, Muraro PA, Daumer M, et al. The natural history of multiple sclerosis: a geographically based study 10: relapses and long-term disability. Brain. 2010;133(Pt 7):1914–29.
85. Trapp BD, Stys PK. Virtual hypoxia and chronic necrosis of demyelinated axons in multiple sclerosis. Lancet Neurol. 2009;8(3):280–91.
86. Raftopoulos R, Hickman SJ, Toosy A, Sharrack B, Mallik S, Paling D, et al. Phenytoin for neuroprotection in patients with acute optic neuritis: a randomised, placebo-controlled, phase 2 trial. Lancet Neurol. 2016;15(3):259–69.
87. Petrova N, Carassiti D, Altmann DR, Baker D, Schmierer K. Axonal loss in the multiple sclerosis spinal cord revisited. Brain Pathol. 2018;28(3):334–48.
88. Evangelou N, Esiri MM, Smith S, Palace J, Matthews PM. Quantitative pathological evidence for axonal loss in normal appearing white matter in multiple sclerosis. Ann Neurol. 2000;47(3):391–5.
89. Wegner C, Esiri MM, Chance SA, Palace J, Matthews PM. Neocortical neuronal, synaptic, and glial loss in multiple sclerosis. Neurology. 2006;67(6):960–7.
90. Popescu V, Klaver R, Voorn P, Galis-de Graaf Y, Knol DL, Twisk JW, et al. What drives MRI-measured cortical atrophy in multiple sclerosis? Mult Scler. 2015;21(10):1280–90.
91. Carassiti D, Altmann DR, Petrova N, Pakkenberg B, Scaravilli F, Schmierer K. Neuronal loss, demyelination and volume change in the multiple sclerosis neocortex. Neuropathol Appl Neurobiol. 2018;44(4):377–90.
92. Zivadinov R, Uher T, Hagemeier J, Vaneckova M, Ramasamy DP, Tyblova M, et al. A serial 10-year follow-up study of brain atrophy and disability progression in RRMS patients. Mult Scler. 2016;22(13):1709–18.
93. Popescu V, Agosta F, Hulst HE, Sluimer IC, Knol DL, Sormani MP, et al. Brain atrophy and lesion load predict long term disability in multiple sclerosis. J Neurol Neurosurg Psychiatry. 2013;84(10):1082–91.
94. Zivadinov R, Havrdova E, Bergsland N, Tyblova M, Hagemeier J, Seidl Z, et al. Thalamic atrophy is associated with development of clinically definite multiple sclerosis. Radiology. 2013;268(3):831–41.
95. Eshaghi A, Prados F, Brownlee W, Altmann DR, Tur C, Cardoso MJ, et al. Deep grey matter volume loss drives disability worsening in multiple sclerosis. Ann Neurol. 2018;83(2):210–22.
96. Filippi M, Preziosa P, Copetti M, Riccitelli G, Horsfield MA, Martinelli V, et al. Gray matter damage predicts the accumulation of disability 13 years later in MS. Neurology. 2013;81(20):1759–67.
97. Bergsland N, Horakova D, Dwyer MG, Uher T, Vaneckova M, Tyblova M, et al. Gray matter atrophy patterns in multiple sclerosis: a 10-year source-based morphometry study. Neuroimage Clin. 2018;17:444–51.
98. Zivadinov R, Dwyer MG, Bergsland N. Brain atrophy measurements should be used to guide therapy monitoring in MS – YES. Mult Scler. 2016;22(12):1522–4.
99. Sormani MP, Arnold DL, De Stefano N. Treatment effect on brain atrophy correlates with treatment effect on disability in multiple sclerosis. Ann Neurol. 2014;75(1):43–9.
100. De Stefano N, Stromillo ML, Giorgio A, Bartolozzi ML, Battaglini M, Baldini M, et al. Establishing pathological cut-offs of brain atrophy rates in multiple sclerosis. J Neurol Neurosurg Psychiatry. 2016;87(1):93–9.
101. Uher T, Vaneckova M, Krasensky J, Sobisek L, Tyblova M, Volna J, et al. Pathological cut-offs of global and regional brain volume loss in multiple sclerosis. Mult Scler. 2019;25(4):541–53.

102. Dwyer MG, Hagemeier J, Bergsland N, Horakova D, Korn JR, Khan N, et al. Establishing pathological cut-offs for lateral ventricular volume expansion rates. Neuroimage Clin. 2018;18:494–501.
103. Sormani MP, Kappos L, Radue EW, Cohen J, Barkhof F, Sprenger T, et al. Defining brain volume cutoffs to identify clinically relevant atrophy in RRMS. Mult Scler. 2018;23(5):656–64.
104. Azevedo CJ, Jaberzadeh A, Pelletier D. New concepts related to disease appreciation in multiple sclerosis. Neurol Clin. 2018;36(1):119–33.
105. Ghione E, Dwyer M, Bergsland N, Hagemeier J, Jakimovski D, Paunkoski I, et al. Normative reference database for lateral ventricular volume change in multiple sclerosis patients. Neurology. 2017;88(16 Suppl):P4.380.
106. Lublin FD, Reingold SC, Cohen JA, Cutter GR, Sorensen PS, Thompson AJ, et al. Defining the clinical course of multiple sclerosis: the 2013 revisions. Neurology. 2014;83(3):278–86.
107. Dwyer MG, Silva D, Bergsland N, Horakova D, Ramasamy D, Durfee J, et al. Neurological software tool for reliable atrophy measurement (NeuroSTREAM) of the lateral ventricles on clinical-quality T2-FLAIR MRI scans in multiple sclerosis. Neuroimage Clin. 2017;15:769–79.
108. Zivadinov R, Bergsland N, Korn JR, Dwyer MG, Khan N, Medin J, et al. Feasibility of brain atrophy measurement in clinical routine without prior standardization of the MRI protocol: results from MS-MRIUS, a longitudinal observational, multicenter real-world outcome study in patients with relapsing-remitting MS. AJNR Am J Neuroradiol. 2018;39(2):289–95.
109. Zivadinov R, Jakimovski D, Gandhi S, Ahmed R, Dwyer MG, Horakova D, et al. Clinical relevance of brain atrophy assessment in multiple sclerosis. Implications for its use in a clinical routine. Expert Rev Neurother. 2016;16(7):777–93.
110. Gareau PJ, Rutt BK, Karlik SJ, Mitchell JR. Magnetization transfer and multicomponent T2 relaxation measurements with histopathologic correlation in an experimental model of MS. J Magn Reson Imaging. 2000;11(6):586–95.
111. Schmierer K, Scaravilli F, Altmann DR, Barker GJ, Miller DH. Magnetization transfer ratio and myelin in postmortem multiple sclerosis brain. Ann Neurol. 2004;56(3):407–15.
112. Arnold DL, Gold R, Kappos L, Bar-Or A, Giovannoni G, Selmaj K, et al. Magnetization transfer ratio in the delayed-release dimethyl fumarate DEFINE study. J Neurol. 2014;261(12):2429–37.
113. Brown RA, Narayanan S, Stikov N, Cook S, Cadavid D, Wolansky L, et al. MTR recovery in brain lesions in the BECOME study of glatiramer acetate vs interferon beta-1b. Neurology. 2016;87(9):905–11.
114. Arnold DL, Calabresi PA, Kieseier BC, Liu S, You X, Fiore D, et al. Peginterferon beta-1a improves MRI measures and increases the proportion of patients with no evidence of disease activity in relapsing-remitting multiple sclerosis: 2-year results from the ADVANCE randomized controlled trial. BMC Neurol. 2017;17(1):29.
115. Rovaris M, Agosta F, Sormani MP, Inglese M, Martinelli V, Comi G, et al. Conventional and magnetization transfer MRI predictors of clinical multiple sclerosis evolution: a medium-term follow-up study. Brain. 2003;126(Pt 10):2323–32.
116. Agosta F, Rovaris M, Pagani E, Sormani MP, Comi G, Filippi M. Magnetization transfer MRI metrics predict the accumulation of disability 8 years later in patients with multiple sclerosis. Brain. 2006;129(Pt 10):2620–7.
117. Fernando KT, Tozer DJ, Miszkiel KA, Gordon RM, Swanton JK, Dalton CM, et al. Magnetization transfer histograms in clinically isolated syndromes suggestive of multiple sclerosis. Brain. 2005;128(Pt 12):2911–25.
118. Brown JW, Pardini M, Brownlee WJ, Fernando K, Samson RS, Prados Carrasco F, et al. An abnormal periventricular magnetization transfer ratio gradient occurs early in multiple sclerosis. Brain. 2017;140(2):387–98.
119. Goodkin DE, Rooney WD, Sloan R, Bacchetti P, Gee L, Vermathen M, et al. A serial study of new MS lesions and the white matter from which they arise. Neurology. 1998;51(6):1689–97.
120. Filippi M, Rocca MA, Martino G, Horsfield MA, Comi G. Magnetization transfer changes in the normal appearing white matter precede the appearance of enhancing lesions in patients with multiple sclerosis. Ann Neurol. 1998;43(6):809–14.
121. Chen JT, Collins DL, Atkins HL, Freedman MS, Arnold DL, Canadian MSBMTSG. Magnetization transfer ratio evolution with demyelination and remyelination in multiple sclerosis lesions. Ann Neurol. 2008;63(2):254–62.
122. Chen JT, Easley K, Schneider C, Nakamura K, Kidd GJ, Chang A, et al. Clinically feasible MTR is sensitive to cortical demyelination in MS. Neurology. 2013;80(3):246–52.
123. Altmann DR, Button T, Schmierer K, Hunter K, Tozer DJ, Wheeler-Kingshott CA, et al. Sample sizes for lesion magnetisation transfer ratio outcomes in remyelination trials for multiple sclerosis. Mult Scler Relat Disord. 2014;3(2):237–43.
124. Schweser F, Deistung A, Reichenbach JR. Foundations of MRI phase imaging and processing for quantitative susceptibility mapping (QSM). Z Med Phys. 2016;26(1):6–34.
125. Haacke EM, Xu Y, Cheng YC, Reichenbach JR. Susceptibility weighted imaging (SWI). Magn Reson Med. 2004;52(3):612–8.
126. Reichenbach JR, Schweser F, Serres B, Deistung A. Quantitative susceptibility mapping: concepts and applications. Clin Neuroradiol. 2015;25(Suppl 2):225–30.

127. Tan IL, van Schijndel RA, Pouwels PJ, van Walderveen MA, Reichenbach JR, Manoliu RA, et al. MR venography of multiple sclerosis. AJNR Am J Neuroradiol. 2000;21(6):1039–42.
128. Maggi P, Absinta M, Grammatico M, Vuolo L, Emmi G, Carlucci G, et al. The central vein sign differentiates MS from CNS inflammatory vasculopathies. Ann Neurol. 2018;83(2):283–94.
129. Hagemeier J, Heininen-Brown M, Gabelic T, Guttuso T Jr, Silvestri N, Lichter D, et al. Phase white matter signal abnormalities in patients with clinically isolated syndrome and other neurologic disorders. AJNR Am J Neuroradiol. 2014;35(10):1916–23.
130. Zivadinov R, Ramasamy DP, Benedict RR, Polak P, Hagemeier J, Magnano C, et al. Cerebral microbleeds in multiple sclerosis evaluated on susceptibility-weighted images and quantitative susceptibility maps: a case-control study. Radiology. 2016;281(3):884–95.
131. Zivadinov R, Heininen-Brown M, Schirda CV, Poloni GU, Bergsland N, Magnano CR, et al. Abnormal subcortical deep-gray matter susceptibility-weighted imaging filtered phase measurements in patients with multiple sclerosis: a case-control study. NeuroImage. 2012;59(1):331–9.
132. Wang Y, Spincemaille P, Liu Z, Dimov A, Deh K, Li J, et al. Clinical quantitative susceptibility mapping (QSM): biometal imaging and its emerging roles in patient care. J Magn Reson Imaging. 2017;46(4):951–71.
133. Chen W, Gauthier SA, Gupta A, Comunale J, Liu T, Wang S, et al. Quantitative susceptibility mapping of multiple sclerosis lesions at various ages. Radiology. 2014;271(1):183–92.
134. Zhang Y, Gauthier SA, Gupta A, Comunale J, Chia-Yi Chiang G, Zhou D, et al. Longitudinal change in magnetic susceptibility of new enhanced multiple sclerosis (MS) lesions measured on serial quantitative susceptibility mapping (QSM). J Magn Reson Imaging. 2016;44(2):426–32.
135. Bagnato F, Hametner S, Yao B, van Gelderen P, Merkle H, Cantor FK, et al. Tracking iron in multiple sclerosis: a combined imaging and histopathological study at 7 Tesla. Brain. 2011;134(Pt 12):3602–15.
136. Hagemeier J, Zivadinov R, Dwyer MG, Polak P, Bergsland N, Weinstock-Guttman B, et al. Changes of deep gray matter magnetic susceptibility over 2 years in multiple sclerosis and healthy control brain. NeuroImage Clin. 2018;18:1007–16.
137. Schweser F, Raffaini Duarte Martins AL, Hagemeier J, Lin F, Hanspach J, Weinstock-Guttman B, et al. Mapping of thalamic magnetic susceptibility in multiple sclerosis indicates decreasing iron with disease duration: a proposed mechanistic relationship between inflammation and oligodendrocyte vitality. Neuroimage. 2018;167:438–52.
138. Mori S, Zhang J. Principles of diffusion tensor imaging and its applications to basic neuroscience research. Neuron. 2006;51(5):527–39.
139. Beaulieu C. The basis of anisotropic water diffusion in the nervous system – a technical review. NMR Biomed. 2002;15(7–8):435–55.
140. Van Essen DC, Smith SM, Barch DM, Behrens TE, Yacoub E, Ugurbil K, et al. The WU-Minn Human Connectome Project: an overview. NeuroImage. 2013;80:62–79.
141. Song SK, Yoshino J, Le TQ, Lin SJ, Sun SW, Cross AH, et al. Demyelination increases radial diffusivity in corpus callosum of mouse brain. NeuroImage. 2005;26(1):132–40.
142. Boretius S, Escher A, Dallenga T, Wrzos C, Tammer R, Bruck W, et al. Assessment of lesion pathology in a new animal model of MS by multiparametric MRI and DTI. NeuroImage. 2012;59(3):2678–88.
143. Rocca MA, Cercignani M, Iannucci G, Comi G, Filippi M. Weekly diffusion-weighted imaging of normal-appearing white matter in MS. Neurology. 2000;55(6):882–4.
144. Calabrese M, Rinaldi F, Seppi D, Favaretto A, Squarcina L, Mattisi I, et al. Cortical diffusion-tensor imaging abnormalities in multiple sclerosis: a 3-year longitudinal study. Radiology. 2011;261(3):891–8.
145. Rocca MA, Sormani MP, Rovaris M, Caputo D, Ghezzi A, Montanari E, et al. Long-term disability progression in primary progressive multiple sclerosis: a 15-year study. Brain. 2017;140(11):2814–9.
146. Cappellani R, Bergsland N, Weinstock-Guttman B, Kennedy C, Carl E, Ramasamy DP, et al. Diffusion tensor MRI alterations of subcortical deep gray matter in clinically isolated syndrome. J Neurol Sci. 2014;338(1–2):128–34.
147. Raz E, Cercignani M, Sbardella E, Totaro P, Pozzilli C, Bozzali M, et al. Clinically isolated syndrome suggestive of multiple sclerosis: voxelwise regional investigation of white and gray matter. Radiology. 2010;254(1):227–34.
148. Benedict RH, Hulst HE, Bergsland N, Schoonheim MM, Dwyer MG, Weinstock-Guttman B, et al. Clinical significance of atrophy and white matter mean diffusivity within the thalamus of multiple sclerosis patients. Mult Scler. 2013;19(11):1478–84.
149. Roosendaal SD, Geurts JJ, Vrenken H, Hulst HE, Cover KS, Castelijns JA, et al. Regional DTI differences in multiple sclerosis patients. NeuroImage. 2009;44(4):1397–403.
150. Preziosa P, Rocca MA, Pagani E, Stromillo ML, Enzinger C, Gallo A, et al. Structural MRI correlates of cognitive impairment in patients with multiple sclerosis: a multicenter study. Hum Brain Mapp. 2016;37(4):1627–44.
151. Pagani E, Hirsch JG, Pouwels PJ, Horsfield MA, Perego E, Gass A, et al. Intercenter differences in diffusion tensor MRI acquisition. J Magn Reson Imaging. 2010;31(6):1458–68.
152. Filippi M, Preziosa P, Rocca MA. Brain mapping in multiple sclerosis: lessons learned about the human brain. NeuroImage. 2019;190:32–45.
153. Reddy H, Narayanan S, Matthews PM, Hoge RD, Pike GB, Duquette P, et al. Relating axonal

injury to functional recovery in MS. Neurology. 2000;54(1):236–9.
154. Rocca MA, Colombo B, Falini A, Ghezzi A, Martinelli V, Scotti G, et al. Cortical adaptation in patients with MS: a cross-sectional functional MRI study of disease phenotypes. Lancet Neurol. 2005;4(10):618–26.
155. Peterson DS, Fling BW. How changes in brain activity and connectivity are associated with motor performance in people with MS. Neuroimage Clin. 2018;17:153–62.
156. Lv H, Wang Z, Tong E, Williams LM, Zaharchuk G, Zeineh M, et al. Resting-state functional MRI: everything that nonexperts have always wanted to know. AJNR Am J Neuroradiol. 2018;39(8):1390–9.
157. Kiviniemi V, Kantola JH, Jauhiainen J, Hyvarinen A, Tervonen O. Independent component analysis of nondeterministic fMRI signal sources. NeuroImage. 2003;19(2 Pt 1):253–60.
158. Tomasi D, Volkow ND. Functional connectivity density mapping. Proc Natl Acad Sci U S A. 2010;107(21):9885–90.
159. Bullmore E, Sporns O. Complex brain networks: graph theoretical analysis of structural and functional systems. Nat Rev Neurosci. 2009;10(3):186–98.
160. Greicius MD, Krasnow B, Reiss AL, Menon V. Functional connectivity in the resting brain: a network analysis of the default mode hypothesis. Proc Natl Acad Sci U S A. 2003;100(1):253–8.
161. Sambataro F, Murty VP, Callicott JH, Tan HY, Das S, Weinberger DR, et al. Age-related alterations in default mode network: impact on working memory performance. Neurobiol Aging. 2010;31(5):839–52.
162. Broyd SJ, Demanuele C, Debener S, Helps SK, James CJ, Sonuga-Barke EJ. Default-mode brain dysfunction in mental disorders: a systematic review. Neurosci Biobehav Rev. 2009;33(3):279–96.
163. Hawellek DJ, Hipp JF, Lewis CM, Corbetta M, Engel AK. Increased functional connectivity indicates the severity of cognitive impairment in multiple sclerosis. Proc Natl Acad Sci U S A. 2011;108(47):19066–71.
164. Rocca MA, Valsasina P, Leavitt VM, Rodegher M, Radaelli M, Riccitelli GC, et al. Functional network connectivity abnormalities in multiple sclerosis: correlations with disability and cognitive impairment. Mult Scler. 2018;24(4):459–71.
165. Rocca MA, Valsasina P, Hulst HE, Abdel-Aziz K, Enzinger C, Gallo A, et al. Functional correlates of cognitive dysfunction in multiple sclerosis: a multicenter fMRI study. Hum Brain Mapp. 2014;35(12):5799–814.
166. Liao X, Vasilakos AV, He Y. Small-world human brain networks: perspectives and challenges. Neurosci Biobehav Rev. 2017;77:286–300.
167. Rocca MA, Valsasina P, Meani A, Falini A, Comi G, Filippi M. Impaired functional integration in multiple sclerosis: a graph theory study. Brain Struct Funct. 2016;221(1):115–31.
168. Friston KJ. Functional and effective connectivity: a review. Brain Connect. 2011;1(1):13–36.
169. Rocca MA, Amato MP, De Stefano N, Enzinger C, Geurts JJ, Penner IK, et al. Clinical and imaging assessment of cognitive dysfunction in multiple sclerosis. Lancet Neurol. 2015;14(3):302–17.
170. Govindaraju V, Young K, Maudsley AA. Proton NMR chemical shifts and coupling constants for brain metabolites. NMR Biomed. 2000;13(3):129–53.
171. Simmons ML, Frondoza CG, Coyle JT. Immunocytochemical localization of N-acetylaspartate with monoclonal antibodies. Neuroscience. 1991;45(1):37–45.
172. Nordengen K, Heuser C, Rinholm JE, Matalon R, Gundersen V. Localisation of N-acetylaspartate in oligodendrocytes/myelin. Brain Struct Funct. 2015;220(2):899–917.
173. Brand A, Richter-Landsberg C, Leibfritz D. Multinuclear NMR studies on the energy metabolism of glial and neuronal cells. Dev Neurosci. 1993;15(3–5):289–98.
174. Sajja BR, Wolinsky JS, Narayana PA. Proton magnetic resonance spectroscopy in multiple sclerosis. Neuroimaging Clin N Am. 2009;19(1):45–58.
175. Lin DD, Crawford TO, Barker PB. Proton MR spectroscopy in the diagnostic evaluation of suspected mitochondrial disease. AJNR Am J Neuroradiol. 2003;24(1):33–41.
176. Kirov II, Liu S, Tal A, Wu WE, Davitz MS, Babb JS, et al. Proton MR spectroscopy of lesion evolution in multiple sclerosis: steady-state metabolism and its relationship to conventional imaging. Hum Brain Mapp. 2017;38(8):4047–63.
177. Narayana PA, Doyle TJ, Lai D, Wolinsky JS. Serial proton magnetic resonance spectroscopic imaging, contrast-enhanced magnetic resonance imaging, and quantitative lesion volumetry in multiple sclerosis. Ann Neurol. 1998;43(1):56–71.
178. Davie CA, Hawkins CP, Barker GJ, Brennan A, Tofts PS, Miller DH, et al. Serial proton magnetic resonance spectroscopy in acute multiple sclerosis lesions. Brain. 1994;117(Pt 1):49–58.
179. De Stefano N, Filippi M, Miller D, Pouwels PJ, Rovira A, Gass A, et al. Guidelines for using proton MR spectroscopy in multicenter clinical MS studies. Neurology. 2007;69(20):1942–52.
180. Ge Y, Gonen O, Inglese M, Babb JS, Markowitz CE, Grossman RI. Neuronal cell injury precedes brain atrophy in multiple sclerosis. Neurology. 2004;62(4):624–7.
181. De Stefano N, Narayanan S, Francis SJ, Smith S, Mortilla M, Tartaglia MC, et al. Diffuse axonal and tissue injury in patients with multiple sclerosis with low cerebral lesion load and no disability. Arch Neurol. 2002;59(10):1565–71.
182. Narayana PA, Wolinsky JS, Rao SB, He R, Mehta M, Group PRTM. Multicentre proton magnetic resonance

spectroscopy imaging of primary progressive multiple sclerosis. Mult Scler. 2004;10(Suppl 1):S73–8.
183. Fleischer V, Kolb R, Groppa S, Zipp F, Klose U, Groger A. Metabolic patterns in chronic multiple sclerosis lesions and normal-appearing white matter: intraindividual comparison by using 2D MR spectroscopic imaging. Radiology. 2016;281(2):536–43.
184. Kirov II, Patil V, Babb JS, Rusinek H, Herbert J, Gonen O. MR spectroscopy indicates diffuse multiple sclerosis activity during remission. J Neurol Neurosurg Psychiatry. 2009;80(12):1330–6.
185. Llufriu S, Kornak J, Ratiney H, Oh J, Brenneman D, Cree BA, et al. Magnetic resonance spectroscopy markers of disease progression in multiple sclerosis. JAMA Neurol. 2014;71(7):840–7.
186. Cocco E, Murgia F, Lorefice L, Barberini L, Poddighe S, Frau J, et al. (1)H-NMR analysis provides a metabolomic profile of patients with multiple sclerosis. Neurol Neuroimmunol Neuroinflamm. 2016;3(1):e185.
187. Lim CK, Bilgin A, Lovejoy DB, Tan V, Bustamante S, Taylor BV, et al. Kynurenine pathway metabolomics predicts and provides mechanistic insight into multiple sclerosis progression. Sci Rep. 2017;7:41473.
188. Hagiwara A, Hori M, Yokoyama K, Takemura MY, Andica C, Tabata T, et al. Synthetic MRI in the detection of multiple sclerosis plaques. AJNR Am J Neuroradiol. 2017;38(2):257–63.
189. West J, Aalto A, Tisell A, Leinhard OD, Landtblom AM, Smedby O, et al. Normal appearing and diffusely abnormal white matter in patients with multiple sclerosis assessed with quantitative MR. PLoS One. 2014;9(4):e95161.
190. Hagiwara A, Warntjes M, Hori M, Andica C, Nakazawa M, Kumamaru KK, et al. SyMRI of the brain: rapid quantification of relaxation rates and proton density, with synthetic MRI, automatic brain segmentation, and myelin measurement. Investig Radiol. 2017;52(10):647–57.
191. Warntjes JB, Leinhard OD, West J, Lundberg P. Rapid magnetic resonance quantification on the brain: optimization for clinical usage. Magn Reson Med. 2008;60(2):320–9.
192. Krauss W, Gunnarsson M, Andersson T, Thunberg P. Accuracy and reproducibility of a quantitative magnetic resonance imaging method for concurrent measurements of tissue relaxation times and proton density. Magn Reson Imaging. 2015;33(5):584–91.